Identification of mesoscale model parameters for brick-masonry

Corrado Chisari[1]*, Lorenzo Macorini[2], Claudio Amadio[3], Bassam A. Izzuddin[4]

Abstract

Realistic assessment of existing masonry structures requires the use of detailed nonlinear numerical descriptions with accurate model material parameters. In this work, a novel numerical-experimental strategy for the identification of the main material parameters of a detailed nonlinear brick-masonry mesoscale model is presented. According to the proposed strategy, elastic material parameters are obtained from the results of diagonal compression tests, while a flat-jack test, purposely designed for in-situ investigations, is used to determine the material parameters governing the nonlinear behaviour. The identification procedure involves: a) the definition of a detailed finite element (FE) description for the tests; b) the development and validation of an efficient metamodel; c) the global sensitivity analysis for parameter reduction; and d) the minimisation of a functional representing the discrepancy between experimental and numerical data. The results obtained by applying the proposed strategy in laboratory tests are discussed in the paper. These results confirm the accuracy of the developed approach for material parameter identification, which can be used also in combination with in-situ tests for assessing existing structures. Practical and theoretical aspects related to the proposed flat-jack test, the experimental data to be considered in the process and the post-processing methodology are critically discussed.

Keywords: Flat-jack test; diagonal compression test; surrogate models; sensitivity analysis; Genetic algorithms.

[1] *(corresponding author) Marie Skłodowska-Curie Research Fellow, Department of Civil and Environmental Engineering, Imperial College London, London SW7 2AZ, United Kingdom, email: corrado.chisari@gmail.com
[2] Senior Lecturer, Department of Civil and Environmental Engineering, Imperial College London, London SW7 2AZ, United Kingdom, email: l.macorini@imperial.ac.uk
[3] Professor of Structural Engineering, Department of Engineering and Architecture, University of Trieste, Piazzale Europa, 1 34127 Trieste, Italy, e-mail: amadio@units.it
[4] Professor of Computational Structural Mechanics, Department of Civil and Environmental Engineering, Imperial College London, London SW7 2AZ, United Kingdom, email: b.izzuddin@imperial.ac.uk

1 Introduction

Masonry is an old material extensively used in the past to construct a variety of structural systems including buildings, bridges and monuments. Thus, most of the historical structures around the world are made of brick- or stone-masonry. Such structures typically exhibit poor performance when subjected to extreme loading (e.g. earthquakes), hence at present they need to be assessed and eventually strengthened to avoid future failures. The behaviour of masonry is very complex, strongly nonlinear and dependent on the properties of the two components, unit and mortar, and their interaction. Therefore, an accurate masonry description allowing for material nonlinearity is generally required to achieve realistic structural response predictions. In the assessment of masonry structures subjected to extreme loading, macroscale models where the characteristics of bricks and mortar joints are smeared into a fictitious continuum or one-dimensional macro-elements (Lourenço, 1996; Berto, et al., 2002; Papa, 1996; Gambarotta & Lagomarsino, 1997; Pantò, et al., 2016) are usually adopted. Although computationally efficient, modelling strategies at the macroscale feature an inherent drawback due to the problematic identification of model material parameters, which should be based on expensive and invasive in-situ experiments. To overcome this limitation, homogenization techniques can be employed to estimate macroscale model parameters from the mechanical characteristics of the constituents (Anthoine, 1995; Mistler, et al., 2007; Milani, et al., 2006; Luciano & Sacco, 1997) or alternatively, approaches explicitly based on separate descriptions of masonry units and mortar joints can be used. Mesoscale masonry models belong to the latter class of modelling strategies, where the contribution of both mortar and brick-mortar interfaces is represented using zero-thickness nonlinear interface elements (Lotfi & Shing, 1994; Lourenço & Rots, 1997; Gambarotta & Lagomarsino, 1997; Macorini & Izzuddin, 2011). This enables the analysis to account also for damage-induced anisotropy achieving realistic predictions of crack propagation within any masonry element. Recent research has shown that the high computational demand generally associated with detailed masonry models can be alleviated by the use of the multi-scale approach (Massart, et al., 2007; Kouznetsova, et al., 2002) and domain decomposition techniques (Park & Felippa, 2000; Jokhio & Izzuddin, 2015; Macorini & Izzuddin, 2013). Thanks to these recent advances in computational mechanics, it seems realistic to predict that mesoscale modelling will be successfully used in the near future also for the analysis of real large-scale masonry structures.

In the case of mesoscale masonry descriptions, model material parameters refer to each masonry component and can be potentially estimated by means of simple material tests (CUR, 1994). However, especially for elastic parameters of interfaces representing mortar joints, it has been shown that correlations with mortar properties obtained from bare mortar samples are generally poor (Chaimoon & Attard, 2007; Da Porto, et al., 2010; Sarhosis, 2016), and intuitive assumptions considering a linear elastic behaviour are not applicable (Lotfi & Shing, 1994; Atkinson, et al., 1989). Moreover, individual components show high scattering in the response (Kaushik, et al., 2007; Brencich & de Felice, 2009), implying that a large number of tests are usually needed to obtain statistically meaningful values. Finally, in the assessment of existing structures it is often difficult to extract specimens to be tested in laboratory, and, in the case of historical buildings, highly invasive testing is not possible at all. To overcome these issues, other methodologies for the calibration of material parameters are required. Instead of performing many tests on small specimens, it can be useful to infer model parameters representative of the "average" structural response by studying larger portions of masonry. In this respect, the use of Inverse Problem Theory (Tarantola, 2005) provides the link between structural behaviour at the macroscale and mesoscale parameters (Fedele, et al., 2006), where inverse methods, considering either static (Morbiducci, 2003;

Sarhosis & Sheng, 2014) or dynamic testing (D'Ambrisi, et al., 2012; Gentile & Saisi, 2007) have been recently applied to the characterisation of masonry models. The application to meso-model calibration was the aim of previous research by the authors (Chisari, et al., 2015), in which an innovative in-situ test was proposed to estimate the elastic properties of the zero-thickness interfaces. The study adopted a pseudo-experimental approach, in which numerical data was perturbed by *a priori* known errors to assess the accuracy of the identification. The setup was subsequently modified and simplified (Chisari, et al., 2015), where elastic parameters were estimated considering the initial loading steps and some nonlinear parameters were identified following an approximate procedure. However, it was later recognised that the estimation of the elastic parameters is strongly affected by the stress state of the test, and the presence of tensile actions may induce premature cracking and consequently inaccurate identification of fictitious "damaged" stiffness. In this paper, an experimental programme in which an inverse analysis procedure is applied to the estimation of the main parameters for a mesoscale masonry model is described. The underlying objective of this investigation is setting up a calibration method for a mesoscale masonry model consisting of a simple and low-invasive experimental test and appropriate post-processing. The proposed approach can be used for the identification of the model material parameters leading to realistic results when the mesoscale description is employed for the assessment of existing masonry structures. In particular, the undamaged elastic parameters are retrieved from the results of diagonal compression tests, while a complete set of parameters governing the nonlinear behaviour is identified fitting the response of a small masonry panel under a purposely designed flat-jack test. The theoretical background, including the material model description and some details of inverse analysis, surrogate modelling and sensitivity analysis are described in Section 2. The experimental programme is presented in Section 3 along with the main outcomes of the physical tests, while the material parameters identification is detailed in Section 4. The conclusions, highlighting the effectiveness of the methodology and indicating future perspectives, are finally drawn in Section 5.

2 Theoretical background

Experimental tests represent a key part of research and professional practice in structural engineering. A crude but incisive taxonomy of experimental testing can be readily associated with the objective of the investigation as follows:

- *Exploration*: no theories exist about the physical process under study, and the outcomes of the tests are used as the basis to understand the phenomenon and the principles underlying it, or directly to the subsequent design/calculation (e.g. in the design assisted by testing allowed by current codes).
- *Validation*: a theory/model must be validated against cases not directly used to develop it.
- *Control*: typical of pre-fabricated structural elements, control testing is used to verify that the products are built according to *a priori* defined prescriptions.
- *Characterisation*: the test provides information about the materials and model parameters. This is in turn used in the response prediction, as for instance in the assessment of existing structures.

Clearly, these categories are not mutually exclusive and overlap. For example, material tests performed during the erection of buildings are at the same time characterisation and control tests, as they are used to verify the consistency between what is being built and the design assumptions. This work concerns with characterization tests which can be described considering:

- the test setup including the instrumentation needed to apply the external actions and the boundary conditions, and all stages of the loading history;
- the data measured in the test. These should be chosen to be as representative as possible of the global response and highly sensitive to the variation of the sought material parameters. An innovative technique for the choice of the experimental data has been recently proposed by the authors (Chisari, et al., 2016) with the aim of recording the most meaningful data for the problem under examination;
- a procedure to post-process the data and provide the results in terms of material parameters, as very seldom the quantities of interest may be directly measured during the test. In traditional tests, this step consists of simple analytical expressions relating the output of the test with the unknown parameters. In tests investigated by inverse analysis, as those described hereinafter, the post-processing involves creating a numerical model of the test and performing an optimisation analysis.

It is often neglected that the parameters estimated by means of a characterisation test always refer to a specific material model. To clarify the concept with a simple example, a diagonal compression test is often used to estimate shear mechanical parameters (Calderini, et al., 2010). These parameters have clearly no meaning if one uses a mesoscale approach to model masonry, where the global strength of the panel depends on the strength properties of the components and the masonry bond.

In the following subsections, all these points are described with reference to an experimental investigation carried out at the Laboratory for Testing Material and Structures at the University of Trieste (Italy).

2.1 The material model

2.1.1 Description of the model

In the masonry model adopted in this work, mortar and brick–mortar interfaces are modelled by 2D 16-noded zero-thickness nonlinear interface elements (Macorini & Izzuddin, 2011). Masonry units are represented by elastic 20-noded solid elements, and possible unit failure in tension and shear is accounted for by means of zero-thickness interface elements place at the vertical mid-plane of each block (Figure 1). The discretisation for the structure, as proposed in (Macorini & Izzuddin, 2011), consists of two solid elements per brick (Figure 1) linked by a brick-brick interface allowing for a possible crack in the brick.

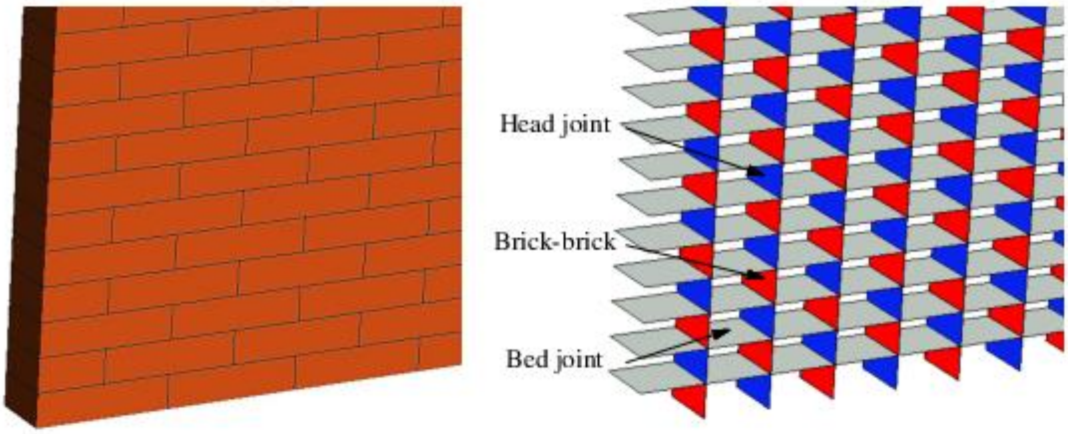

(a) (b)

Figure 1. Mesoscale representation for brick-masonry.

The interface local material model is formulated in terms of one normal and two tangential tractions **σ** (1) and relative displacements **u** (2) evaluated at each integration point over the reference mid-plane:

$$\boldsymbol{\sigma} = \{\tau_x, \tau_y, \sigma\}^T \quad (1)$$

$$\boldsymbol{u} = \{u_x, u_y, u_z\}^T \quad (2)$$

The constitutive model for zero-thickness interfaces considers specific elastic stiffness values which are regarded as uncoupled:

$$\boldsymbol{k_0} = \begin{bmatrix} k_V & 0 & 0 \\ 0 & k_V & 0 \\ 0 & 0 & k_N \end{bmatrix} \tag{3}$$

In Equation (3), k_N and k_V are respectively the normal and the tangential stiffness, the latter assumed equal in the two main directions in the local plane *xy*.

The formulation for nonlinear behaviour is characterized by one hyperbolic yield function F_1 to simulate Mode I and Mode II fracture, providing smooth transition between pure tension and shear failure:

$$F_1 = \tau_x^2 + \tau_y^2 - (c - \sigma\ tan\phi)^2 + (c - \sigma_t\ tan\phi)^2 = 0 \tag{4}$$

The three parameters c, σ_t, $tan\phi$ associated with surface F_1 represent cohesion, tensile strength and friction coefficient at mortar interface. A hyperbolic plastic potential different from the yield function is considered to avoid excessive dilatancy and account for the actual roughness of the fracture surface. The model employs a second hyperbolic function F_2, the cap in compression, to account for crushing in the mortar interfaces. It must be only mentioned here that more advanced mesoscale models representing the actual nonlinear behaviour under compressive failure of masonry exist (Xavier, et al., 2013), but this type of failure is not taken into account in this work. Furthermore, both surfaces F_1 and F_2 shrink with the development of plastic work, following an evolution law governed by the fracture energy, which is assumed as characteristic property of the material. Three fracture energies are to be defined to fully characterise the nonlinear response of the interface: $G_{f,I}$ for mode I (tension) failure, $G_{f,II}$ for mode II (shear) failure, and $G_{f,C}$ for failure in compression. It is assumed that when the dissipated energy equals the fracture energy cohesion, tensile strength and friction coefficient reach some residual values, characteristic of the material. Further details of this model, which is implemented in ADAPTIC (Izzuddin, 1991), are provided elsewhere (Macorini & Izzuddin, 2011).

2.1.2 Physical meaning of model parameters

Lumping mortar joints into zero-thickness interfaces and extending the solid elements representing bricks have important effects on the definition of the elastic parameters. With reference to the stress state shown in Figure 2a, the shortening Δu of the element of length h_b+h_m is:

$$\Delta u = \sigma\left(\frac{h_m}{E_m} + \frac{h_b}{E_b}\right) \tag{5}$$

where E_m, E_b are mortar and brick Young modulus respectively. In the mesoscale representation (Figure 2b), Δu reads:

$$\Delta u = \sigma\left(\frac{1}{k_N} + \frac{h_b + h_m}{E_b}\right) \tag{6}$$

where now k_N is the zero-thickness interface axial stiffness. Imposing the congruence between the two representations, we obtain the expression:

$$k_N = \frac{E_m E_b}{h_m(E_b - E_m)} \tag{7}$$

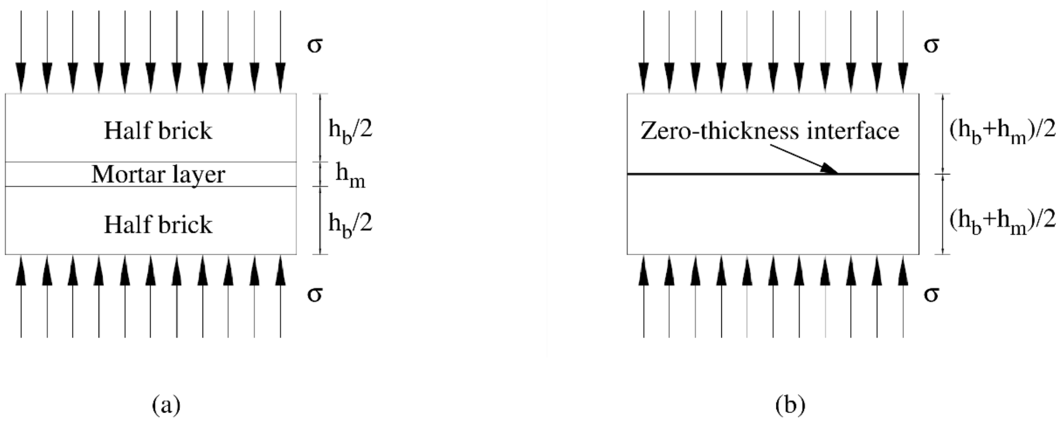

Figure 2. (a) Simple brick-mortar element subjected to compression, and (b) mesoscale representation.

Considering on the other hand a shear stress state, the analogous expression for the shear stiffness can be obtained as:

$$k_V = \frac{G_m G_b}{h_m(G_b - G_m)} \quad (8)$$

Equations (7) and (8) are suggested in (Lourenço, 1996) and (CUR, 1994) for the calibration of interface stiffness values. From these equations, it is clear that the stiffness value is not a mortar characteristic "per-se" but it contains information about the relationship between mortar and brick Young modulus. It is not recommended thus to consider the stiffness value as unknown in the identification problem, as in the numerical study (Chisari, et al., 2015), but rather consider separately E_m and E_b and then estimate k_N and k_V by means of Equations (7) and (8). A very high interface stiffness does not correspond to a very stiff mortar joint, but simply to similar Young's moduli of the masonry components. Equations (7) and (8) are not defined when $E_m \geq E_b$. In this case, to maintain compatibility between the two representations, keeping the interface stiffness equal to infinity, an increase in the fictitious brick Young's modulus E_{bf} in Figure 2b must correspond to an increase in E_m in Figure 2a. Considering the equality between Equations (5) and (6) with $1/k_N$=0, E_{bf} reads:

$$E_{bf} = E_b \frac{h_m + h_b}{h_m \frac{E_b}{E_m} + h_b} \quad (9)$$

and, in this case, the equivalence between unit Young modulus E_{bf} in the mesoscale model and experimental brick Young's modulus E_b does not hold anymore. Analogously, $G_{bf} = G_b \frac{H}{h_m \frac{G_b}{G_m} + h_b}$, and the Poisson's ratio may be defined as $\nu_{bf} = {E_{bf}}/{2G_{bf}} - 1$.

Another interesting consideration arises if we consider the ratio between k_N and k_V defined as in Equations (7) and (8):

$$\frac{k_N}{k_V} = 2 \cdot (1 + \nu_i) \quad (10)$$

with $\nu_i = \frac{\nu_m - {E_m}/{E_b}\nu_b}{1-{E_m}/{E_b}}$. It is evident that, ν_i may in some case assume negative values also when satisfying the condition $E_m<E_b$ (where equations (7) and (8) are defined), meaning that the axial stiffness may even be smaller than the shear stiffness. This was reported in (Lotfi & Shing, 1994) from experimental observations. As a further complication, the definition of the mortar Poisson's ratio is never straightforward, since as highlighted in (McNary & Abrams, 1985) it strongly depends upon the stress state. Thus, ν_m often assumes a "conventional" value, and this once more shows the limitations of considering a linear elastic behaviour for masonry.

Regarding the mortar strength properties, UNI EN 1052 (UNI EN 1052-3:2007, 2007) provides a reference for determining initial shear strength (cohesion) and friction angle from tests on triplets. It implicitly assumes a linear relationship, determined by means of linear regression of the experimental data, between compressive stress and shear strength (Mohr-Coulomb law). Furthermore, the peak shear stress is evaluated as mean stress, i.e. assuming a constant stress distribution at failure. Both assumptions may not be valid for the material model utilised in this work. Equation (4) defines a hyperbolic curve with asymptote characterised by the slope $tan\phi$, meaning that the linear relationship between shear and axial stress assumed by the standard is reasonable only asymptotically, i.e. for high values of compression. Cohesion, which in the approach (UNI EN 1052-3:2007, 2007) is the value of the yield function for zero compressive stress, represents the intercept of the *asymptote* with the axis $\sigma = 0$ in the mesoscale model, whereas the actual intercept of F_1 assumes a different value. The hyperbolic curve reduces to a straight line only when $c = \sigma_t = 0$, as it is usually observed at residual state. In addition, it seems at least doubtful that in the shear test a stress redistribution could manifest, given the brittleness usually reported. So, the evaluation of the peak shear stress as mean stress may not be consistent with the stress state given at peak by a mesoscale representation. For this reason, special care should be taken to identifying the strength parameters c and $tan\phi$ in Equation (4) with the corresponding “cohesion” and “friction coefficient” obtained by ordinary post-processing the results from shear tests on triplets.

2.1.3 Some assumptions on the nonlinear parameters

The set of parameters controlling the nonlinear behaviour of the mortar interfaces include cohesion, friction angle and tensile strength for the initial and residual state, dilatancy angle, parameters controlling the compressive failure surface, and fracture energies for all the different failure modes. Furthermore, these parameters should be defined for three types of interfaces, modelling bed and head joints and brick-brick cracks, respectively. It is not realistic to identify all parameters by means of a single test; so, to decrease the number of unknowns for the inverse procedure, some assumptions must be made.

Firstly, for bed joints it is common practice to assume the same friction angle for the initial and residual state, and zero residual cohesion (Atkinson, et al., 1989); this also implies zero residual tensile strength. Secondly, due to lack of significant normal stress, shrinkage and the subsequent loss of bond between the unit and mortar, the contribution of the head joints to the shear transfer is considered insignificant by many authors, compared to that of the bed joints (Mann & Muller, 1982; Ganz, 1985; Mojsilovic & Marti, 1997). Consequently, even initial cohesion and tensile strength have been neglected for the head joints, while the friction coefficient has been set equal to that of bed joints. Furthermore, no dilatancy has been considered and, as compressive strength is not of concern in this investigation and neither may be estimated by means of the proposed test, it was set as very high, and so was the fracture energy in compression (for both mortar and brick-brick interfaces). Finally, as shear failure is rarely significant in bricks, cohesion and friction angle for the brick-brick interface assumes a conventional value, whereas the most important parameters are those related to mode-I failure.

All these assumptions allow for decreasing the number of unknowns to the following:

- cohesion c, tensile strength σ_t for the bed joints;
- friction coefficient $tan\phi$ for bed and head joints;
- fracture energies $G_{f,I}$ and $G_{f,II}$ for bed and head joints;
- tensile strength f_{tb} and mode-I fracture energy $G_{fb,I}$ for brick-brick interfaces.

2.2 Calibration through inverse analysis

2.2.1 Overview

Physical theories allow us to make predictions, hence given a complete description of a physical system, we can predict the outcome of some measurements $\boldsymbol{d_c}$ (forward problem). The solution of the system of partial differential equations describing the process can be approximated using a FE model. The inverse problem consists of using the actual result of some measurements $\boldsymbol{d_{obs}}$ to infer the values of the parameters $\boldsymbol{m}$ characterising the system. Due to measurement uncertainties and modelling imperfections, the predicted values generally cannot be identical to the observed values. Hence, the calibration problem is solved by minimising:

$$\widetilde{\boldsymbol{m}} = \arg\min_{\boldsymbol{m}} \omega\big(\boldsymbol{d_{obs}}, \boldsymbol{d_c}(\boldsymbol{m})\big) \tag{11}$$

where $\widetilde{\boldsymbol{m}}$ is the solution of the optimisation problem, ω is the discrepancy (or cost) function, measuring the inconsistency between $\boldsymbol{d_{obs}}$ and $\boldsymbol{d_c}$, the latter depending on the unknown material parameters $\boldsymbol{m}$. The general formulation for the discrepancy function is:

$$\omega(\boldsymbol{d_{obs}}, \boldsymbol{d_c}(\boldsymbol{m})) = \left(\| \boldsymbol{d_{obs}} - \boldsymbol{d_c}(\boldsymbol{m})\|_q\right)^q \tag{12}$$

where $\|\cdot\|_q$, with $1 \leq q \leq \infty$, is the weighted L_q-norm of a vector. The most common formulation is given with q=2 (Euclidean norm), and it is derived directly from the assumption that all measurements follow a Gaussian probability distribution (Tarantola, 2005). If gross errors (outliers) are expected, it is preferable to impose q=1, i.e. the Least-Absolute-Value criterion in Equation (12) (Claerbout & Muir, 1973).

Applied to structural problems, the identification process implies performing an experimental test, from which some observed data $\boldsymbol{d_{obs}}$ are recorded, and a numerical simulation of the test to calculate the corresponding numerical results $\boldsymbol{d_c}$. The solution of the optimisation problem, where the discrepancy between the two sets of data is minimised, gives the sought material parameters $\boldsymbol{m}$. To solve the optimisation problem (11), several methods can be used. Even though gradient-based methods are computationally attractive, Genetic Algorithms (Goldberg, 1989) are more effective in many cases, as they do not require calculating derivatives, and allow overcoming potential numerical problems associated with non-convex and non-continuous objective functions. In this respect, they were used for kinematic limit analysis of complex masonry components, e.g. vaults in (Chiozzi, et al., 2017), and optimal design of structures (Poh'sie, et al., 2016; Chisari & Bedon, 2016). In this work, a GA implemented in the software TOSCA (Chisari, 2015) has been employed.

In some cases, before performing inverse analysis, a preliminary stage involving metamodel construction-validation and model parameter reduction is required. This is the topic of the next subsections.

2.2.2 The Kriging surrogate model

One of the bottlenecks of the optimisation process is the large number of forward analyses needed to solve problem (11), often in the order of hundreds if not thousands. Thus to guarantee a reasonable overall computing time, the single analysis should take some seconds or a very few minutes at most. This could potentially limit the possibility of using the framework described before, as nonlinear analyses of complex 3D models may require hours in many cases. To address this issue, a possible strategy consists of using metamodels (or surrogate models) to approximate the solution of the finite element model. A similar concept was considered in (Milani & Benasciutti, 2010), where polynomial Response Surface approximation was adopted for expensive Monte Carlo simulations of masonry structures.

In general, if the FE model represents a black-box functional $\boldsymbol{d_c}=F(\boldsymbol{m})$ which gives the numerical response for a trial choice of material parameters $\boldsymbol{m}$, a metamodel is "model of the model", i.e. a known function $\widetilde{\boldsymbol{d}}_c = \tilde{F}(\boldsymbol{\vartheta}, \boldsymbol{m})$ which provides an approximated response $\widetilde{\boldsymbol{d}}_c$ depending on the material parameters $\boldsymbol{m}$ and some metamodel parameters $\boldsymbol{\vartheta}$. The latter parameters are calibrated such as the approximate response $\widetilde{\boldsymbol{d}}_c$ fits exactly the "true" response $\boldsymbol{d_c}$ at some design points. Thus, the construction of a metamodel implies (i) an off-line phase, in which the complex numerical model is evaluated at the design points (calibration set) calculating the parameters $\boldsymbol{\vartheta}$, and (ii) a validation phase in which the true and approximate responses for different points in a validation set are compared. If the chosen statistics (i.e. mean, maximum) of the error in the validation set satisfy a certain criterion, the metamodel may be employed in place of the detailed model to obtain a fast-computed response; otherwise, the number of design points must be increased or the metamodel changed.

Several classes of metamodels exist in the literature (Press, et al., 2007), among which very popular are Radial Basis Functions and quadratic or cubic Response Surfaces. Although rather powerful to approximate nonlinear black-box functionals, these approaches requires inversion of matrices which can easily become ill-conditioned when, due to large number of variables, equi-spaced grids for the design points are not suitable, and random or quasi-random sequences must be used instead. An effective class of metamodels which solves this drawback is represented by the kriging methods, widely utilised in geostatistics. Named after the South-African mining engineer D.G. Krige, this class of methods consists of approximating the function value by a weighted sum of the known data, but, unlike other approximating techniques, which assign decreasing weights with increasing separation distance, kriging assigns weights according to a (moderately) data-driven weighting function. Considering for the sake of simplicity the case in which a single response d is to be approximated, the method considers the function $d(\boldsymbol{m})$ as a random field with a trend component, $t(\boldsymbol{m})$, and a residual component, $R(\boldsymbol{m}) = d(\boldsymbol{m}) - t(\boldsymbol{m})$. The estimator $\tilde{d}(\boldsymbol{m})$ is defined as:

$$\tilde{d}(\boldsymbol{m}) = \mathcal{F}(\boldsymbol{\beta}, \boldsymbol{m}) + z(\boldsymbol{\theta}, \boldsymbol{m}) \tag{13}$$

where:

- $\tilde{d}(\boldsymbol{m})$ is the estimated value of the function at location $\boldsymbol{m}$;
- $\mathcal{F}(\boldsymbol{\beta}, \boldsymbol{m})$ is the regression model, which approximates the trend component $t(\boldsymbol{m})$;
- $z(\boldsymbol{\theta}, \boldsymbol{m})$ is the random process which approximates the residual $R(\boldsymbol{m})$.

The regression model $\mathcal{F}(\boldsymbol{\beta}, \boldsymbol{m})$ is defined as linear combination of p chosen functions, through the coefficients $\boldsymbol{\beta}$, called regression parameters. The random process $z(\boldsymbol{\theta}, \boldsymbol{m})$, assumed to have zero mean and covariance $E\left[d(\boldsymbol{m_i})d\left(\boldsymbol{m_j}\right)\right] = \sigma^2\mathcal{R}(\boldsymbol{\theta}, \boldsymbol{m_i}, \boldsymbol{m_j})$ with σ^2 process variance for *d*, depends on a correlation model $\mathcal{R}(\boldsymbol{\theta}, \boldsymbol{m_i}, \boldsymbol{m_j})$ with parameters $\boldsymbol{\theta}$. The correlation model is usually selected as dependent on the distance $\boldsymbol{r} = \boldsymbol{m_i} - \boldsymbol{m_j}$, i.e. $\mathcal{R} = \mathcal{R}(\boldsymbol{\theta}, \boldsymbol{m_i} - \boldsymbol{m_j})$. Given some design points, the regression parameters $\boldsymbol{\beta}$ are evaluated by imposing that, under the unbiasedness constraint $E\left\{d(\boldsymbol{m}) - \tilde{d}(\boldsymbol{m})\right\} = 0$, the mean squared error of the linear predictor is minimised. This consists of solving a generalised least squares problem with respect to *R*, the matrix of stochastic-process correlations between $\boldsymbol{m}$ at the design points. Hence, a preliminary choice of the parameters $\boldsymbol{\theta}$ must be made: following (Lophaven, et al., 2002), the optimal choice $\boldsymbol{\theta}^*$is selected as the maximum likelihood estimator. In this work, the DACE toolbox (Lophaven, et al., 2002) is utilised to build the surrogate model of the nonlinear numerical FE model. More details on the theoretical aspects and issues can be found elsewhere (Lophaven, et al., 2002; Lophaven, et al., 2002).

2.2.3 Sensitivity analysis

To fully define the numerical model used in the optimisation process, many parameters describing material properties or boundary conditions are usually needed. As the experimental data available are usually limited and thus the inferred information is necessarily incomplete, it may be necessary to reduce the number of unknowns of the inverse problem to those which are actually possible to estimate.

To understand which model parameters are important in a test response and which ones conversely have little influence, a preliminary global sensitivity analysis (SA) is needed: the method of elementary effects (EE) (Morris, 1991), belonging to the class of screening methods, is considered in the following. The EE method is a screening method aiming at determining if the effect of each parameter is a) negligible, b) linear and additive, c) nonlinear or involved in interactions with other inputs, with a reasonable computational effort (remarkably lower than Monte Carlo-based methods). It implies that interactions among parameters are detected only in a qualitative fashion. The method is based on the evaluation of the elementary effect EE_i of the parameter m_i on the scalar response $d(\boldsymbol{m})$ when it is perturbed by a step Δ_i while all the other parameters are fixed. It is defined as:

$$EE_i = \frac{d(m_1, \dots, m_{i-1}, m_i + \Delta_i, m_{i+1}, \dots, m_k) - d(m_1, \dots, m_k)}{\Delta_i} \tag{14}$$

with k number of parameters.

The global sensitivity measure is the finite distribution F_i composed of all possible EE_i. It may be represented by the values of the mean and standard deviation, estimated from a sample composed by N points:

$$\begin{gathered} \mu_i = \frac{1}{N}\sum_{i=1}^{N} EE_i \\ \sigma_i = \sqrt{\frac{1}{N-1}\sum_{i=1}^{N}(EE_i - \mu_i)^2} \end{gathered} \tag{15}$$

A large measure of central tendency μ_i for F_i indicates an input with important "overall" influence on the output. A large measure of spread σ_i indicates an input whose influence is highly dependent on the values of the overall set of inputs, meaning that it is involved in interactions with other parameters or its effect is nonlinear. The sensitivity analyses is performed here by means of the SAFE toolbox (Pianosi, et al., 2015).

The whole calibration process is shown in Figure 3.

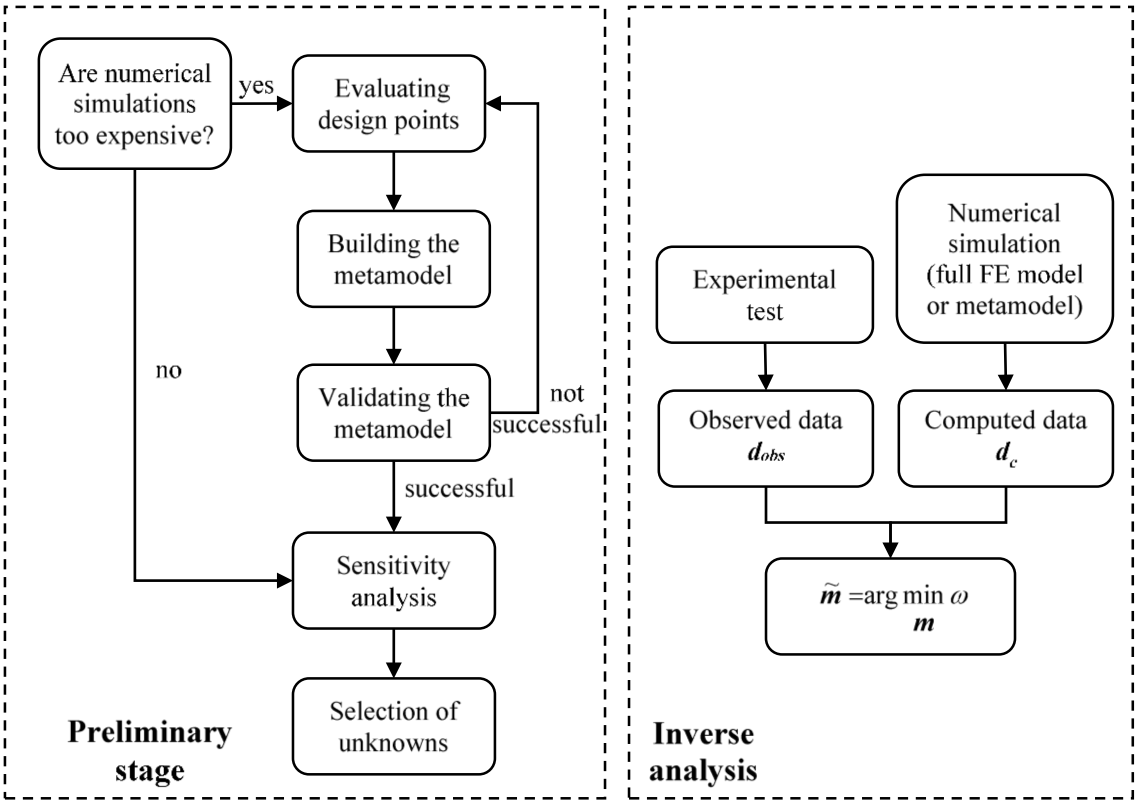

Figure 3. The identification process.

3 The experimental programme

The procedure illustrated in the previous section has been used to determine the mesoscale material characteristics of masonry specimens physically tested in an experimental programme including diagonal compression and flat-jacks tests as discussed in the following. The material were nominally the same for all tests performed. The masonry specimens were built using M4 mortar with 1:1:5 (cement:lime:sand) proportion by volume with assumed characteristic compressive strength at 28 days equal to 4 N/mm^2 (BS 5628-1: 2005, 2005). The units were 250×120×55mm^3 clay bricks. Standard material and small specimen tests were performed to obtain some initial reference values for the masonry material properties. These tests include: 1) compressive (a) and splitting (b) tests on mortar cylinders; 2) compressive (a) and splitting (b) tests on bricks; 3) compressive tests on stack-bond masonry prisms and 4) shear tests on masonry triplets. The test results are reported in Table 1, along with the coefficients of variation (CV).

Table 1. Material properties of the tested masonry wall.

Test	**Property**	**Symbol**	**Average**	**CV**
1a	Mortar compressive strength	f_m	7.86 MPa	6.24%
1b	Mortar tensile strength	f_{vm}	1.33 MPa	31.79%
2a	Brick compressive strength	f_b	18.27 MPa	14.08%
2b	Brick tensile strength	f_{tb}	4.233 MPa	3.94%
2a	Brick Young modulus	E_b	11.2 GPa	16.28%
2a	Brick Poisson ratio	ν_b	0.19	35.71%
3	Masonry compressive strength	f_s	18.98 MPa	22.62%
3	Masonry Young modulus	E_s	6.9 GPa	20.58%
4	Mortar-brick interface peak cohesion	c_p	0.298 MPa	26.11%
4	Mortar-brick interface residual cohesion	c_r	0.046 MPa	91.33%
4	Mortar-brick interface peak friction coefficient	$tan\phi_p$	1.579	9.30%
4	Mortar-brick interface residual friction coefficient	$tan\phi_r$	1.135	6.61%

3.1 The diagonal compression test

Two 650×650×90mm^3 running bond wallettes (labelled CD1 and CD2) were tested under diagonal compression. The panels were made of 250×55×90 mm^3 solid clay bricks, 10 mm thick mortar bed joints and mortar head joints with 15 mm thickness. The results from material tests are reported in Table 1. Before the test, each panel was rotated and placed on a stiffened steel angle, and a similar angle was set at the opposite top corner for the load application. Thin layers of plaster and sand were arranged between the two steel angles and the specimen to enable the development of a uniform distribution of stresses during the test (Figure 4a).

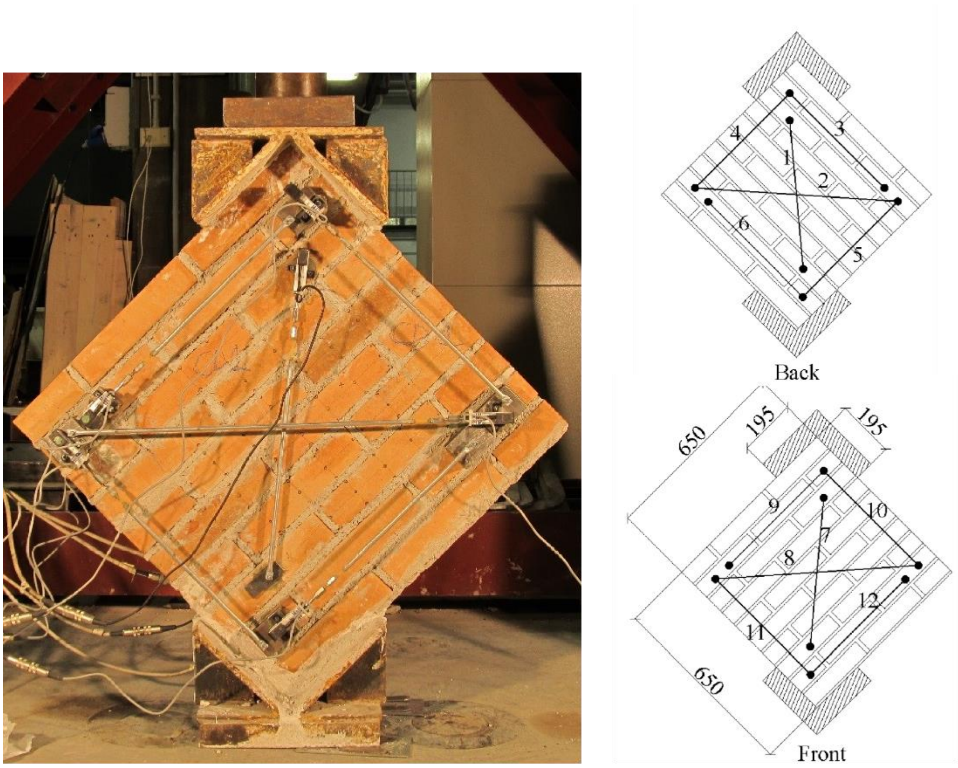

(a) (b)

Figure 4. Diagonal compression test: (a) lateral view and (b) sensor position.

Displacements were acquired by 12 LVDTs (25mm stroke) on both specimen faces along the diagonals and the specimen edges (Figure 4b). Aluminium bars were used to connect each LVDT to the opposite gauge point. The load was applied by a hydraulic jack with 200kN maximum load. As the test was force-controlled, the post-peak behaviour was not captured.

3.2 The flat-jack test

The proposed experimental setup consists of a non-conventional shear test proposed in other context by (Caliò, 2011), in which a vertical flat-jack is used to apply a controlled pressure on the surrounding masonry (Figure 5a). This gives rise to a displacement field, whose investigation allows estimating strength properties of mortar joints when cracks begin to develop. This set-up can be used also for in-situ experiments, where vertical stresses on the portion of the tested masonry panel, which influence masonry strength, can be preliminarily estimated by a conventional flat-jack test (ASTM, 1991).

The physical test was performed in laboratory on a 1310×1960×120mm^3 running bond masonry wall, made up of 250×120×55 mm^3 bricks, 10 mm thick horizontal mortar bed joints and 15 mm thick mortar head joints, using the same masonry components and bond of the masonry walletes tested under diagonal compression. The slot for the vertical flat-jack was prepared during the construction phase and filled with polystyrene sheets, to avoid cutting the panel. To be consistent with a potential in-situ application, a horizontal flat-jack was used to estimate vertical stresses induced by a hydraulic jack and distributed by a steel beam on the top of the panel. The adopted 240×120×4 mm^3 rectangular flat-jacks are manufactured by DRC (DRC Diagnostic Research Company, 2015) and are characterised by 60 bar maximum admissible pressure. The effective pressure p_{vfj} transferred by the flat-jack may be evaluated as:

$$p_{vfj} = K_m \cdot K_a \cdot p \tag{16}$$

where p is the pressure in the flat-jack measured by the gauge, K_m is a constant provided by the manufacturer and equal to 0.86. K_a is the area factor depending on size of the slot which is 250mm wide, thus K_a=240/250=0.96.

The vertical flat-jack pressure induces high shear stresses in the mortar bed joints and tensile stress in the adjacent bricks (Figure 5b). Depending on the relative strength of the two components and the geometrical configuration of the specimen, increasing pressure can lead either the brick or the mortar to fail. To avoid tension failure with propagation of vertical cracks without significant development of material nonlinearity in mortar bed joints, the bricks above and below the vertical flat-jack were reinforced using Carbon Fibre-Reinforced Polymer (CFRP) strips, as shown in Figure 5c.

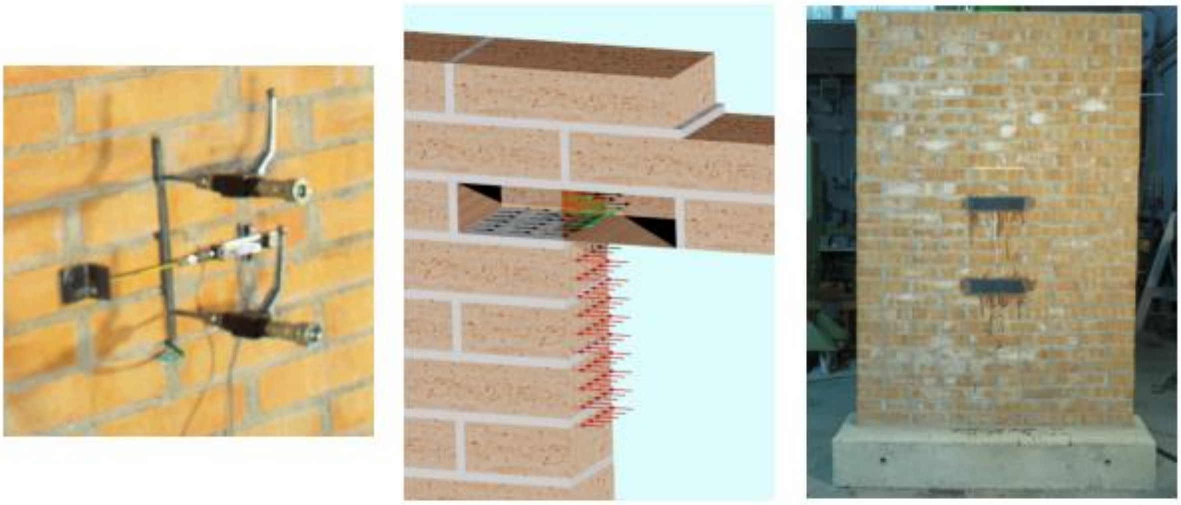

(a) (b) (c)

Figure 5. Flat-jack test: (a) Application of the flat-jack, (b) qualitative stress state near the cutting, and (c) view of the specimen with FRP reinforcement.

The displacement field was measured by 18 LVDTs with 25 mm stroke. Eleven of these were used to obtain displacement data around the vertical flat-jack (Figure 6a) considering two groups: (a) those in proximity of the vertical slots (Figure 6b), and those with larger base length (Figure 6c). The sensor placement was designed mainly following the procedure described in (Chisari, et al., 2016) introducing some modifications based on the experimental observations, as discussed in the next parts.

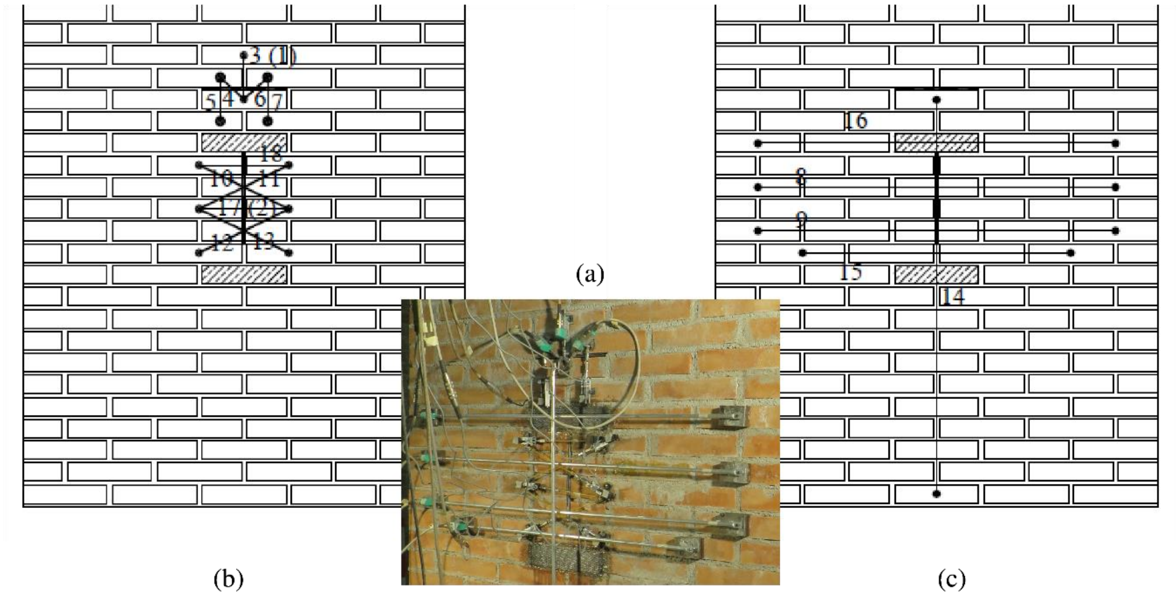

Figure 6. Instrumentation for displacement acquisition from the flat-jack test: (a) view of the setup around the vertical flat-jack; (b) LVDTs in proximity of the vertical slot; (c) LVDTs with longer base length.

3.3 Experimental results

3.3.1 Diagonal test

The results of the two diagonal compression tests are summarised in Figure 7, where the curves represent the average between the measurements on the two sides of the specimen: LVDTs 1,7 for the principal diagonal and 2,8 for the secondary diagonal, with reference to Figure 4. The ultimate load for specimen CD1 was equal to 144.95kN and to 173.10kN for specimen CD2.

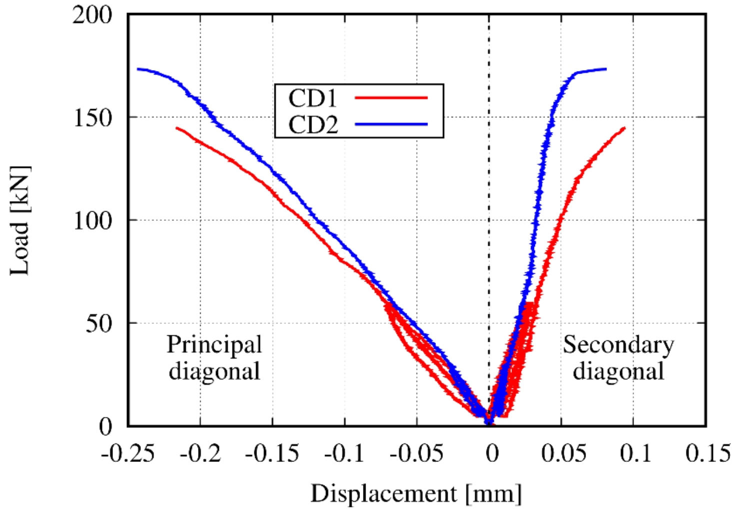

Figure 7. Load-displacement curves for the diagonal compression tests.

The failure modes are shown in Figure 8. In particular, specimen CD1 was characterised by failure of the mortar-brick interface along bed and head joints and limited cracks in the bricks. On the contrary, CD2 exhibited vertical cracks intersecting both bricks and mortar.

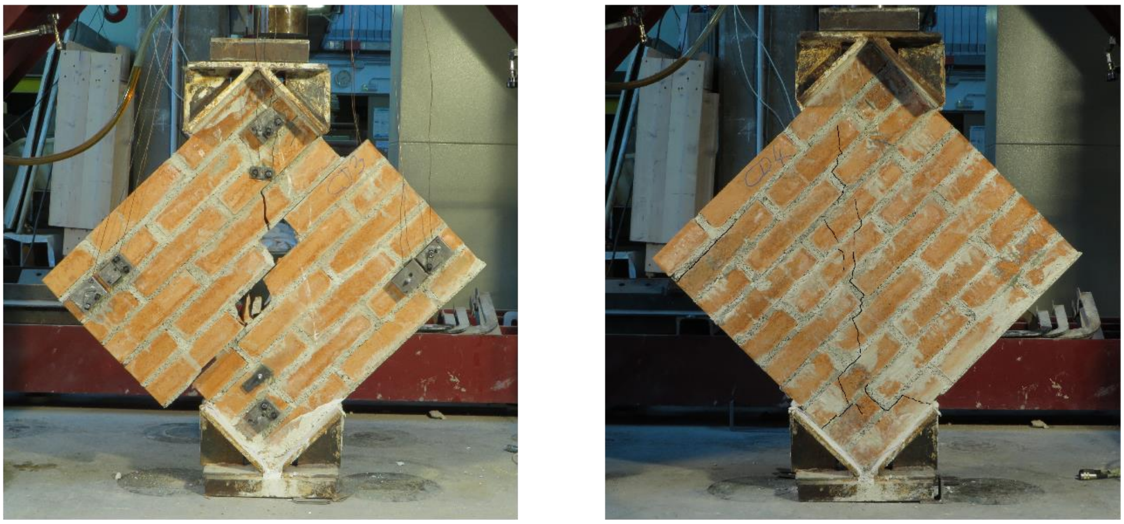

(a) (b)

Figure 8. Failure modes for the diagonal compression tests on specimens (a) CD1 and (b) CD2.

3.3.2 Flat-jack test

The results in terms of the load-displacement curve of a representative LVDT placed at the middle of the slot (LVDT 2) are shown in Figure 9. The maximum load transferred by the vertical flat-jack was equal to 3.65MPa. After reaching the peak, the load gradually decreased under increasing displacements until reaching an almost horizontal plateau at a pressure equal to about 2.60MPa.

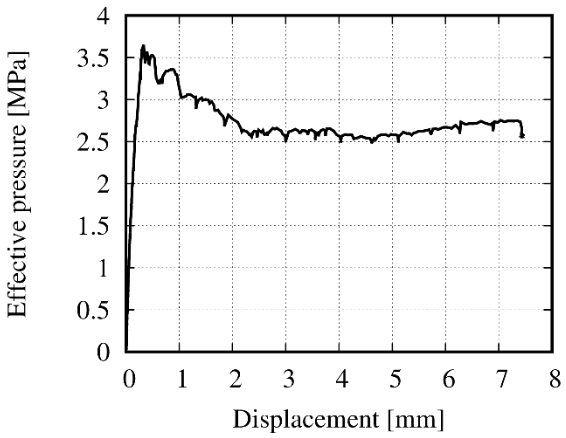

Figure 9. Load-displacement plot of LVDT 2 in the flat-jack test.

At failure, diagonal cracks developed in the upper-right part of the specimen (Figure 10a). Because of the CFRP reinforcement, cracks developed vertically just below the reinforced brick until the base of the specimen. Even though the cracking pattern was clearly asymmetric, symmetric diagonal cracks in the bricks close to the vertical slot were observed. Some of them eventually developed into major cracks characterising the ultimate behaviour.

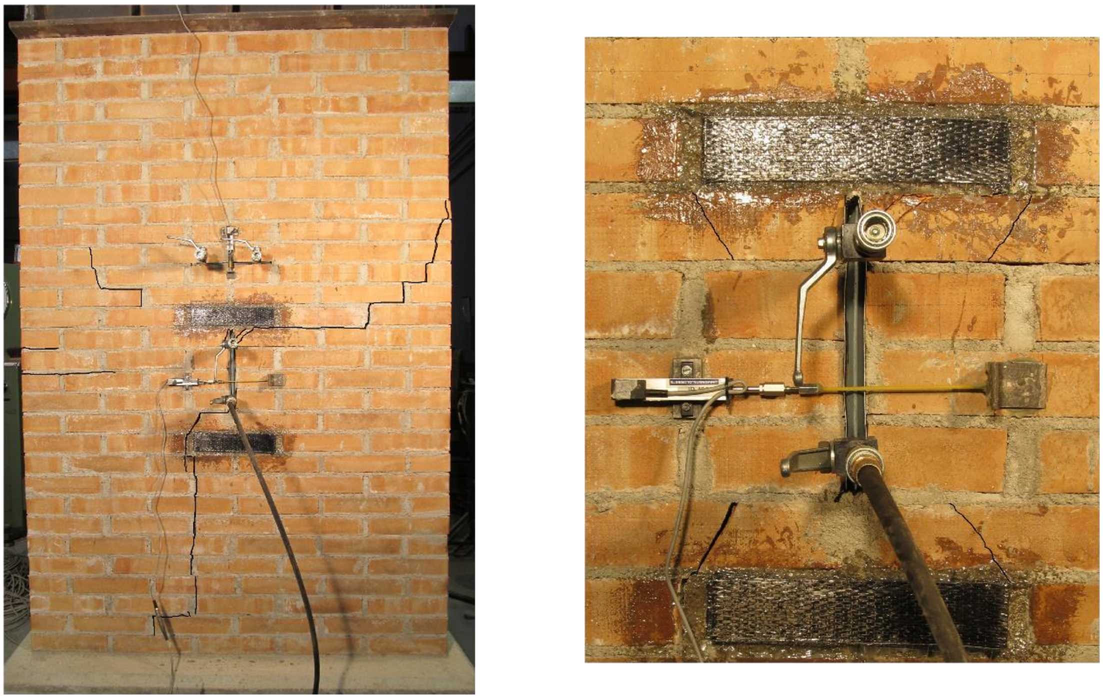

(a) (b)

Figure 10. Flat-jack test: (a) the specimen at failure with major cracks, and (b) minor cracks around the slot.

It is important to point out that the post-elastic behaviour of the proposed flat-jack test is remarkably ductile, especially compared to the diagonal compression test. This is an important feature for a test used for the calibration of material parameters governing the nonlinear behaviour for two reasons. Firstly, a brittle failure, as that exhibited by the diagonal compression test, is likely to be triggered by local defects. Thus, large scattering is expected in the results, as confirmed by the different ultimate loads of the two specimens made of the same materials, and a considerable number of test repetitions is generally needed to obtain an averaged response for the masonry. Furthermore, a ductile behaviour with relatively large deformations is generally due to the contribution of a larger number of material parameters, including fracture energy, which do not play a significant role in the first stages of the nonlinear response.

4 Identification of model parameters

4.1 Elastic parameters

4.1.1 Issues in identification of elastic properties

A typical approach to the identification of a complete set of model parameters usually consists of splitting the problem into two sub-problems (Sarhosis & Sheng, 2014; Chisari, et al., 2015; Garbowski, et al., 2011): i) estimation of elastic properties considering the initial part of the experimental plots and a linear model for the numerical simulations, and ii) estimation of nonlinear properties after fixing the previously calibrated elastic parameters. Although this methodology may appear reasonable in some contexts, it may lead to substantial errors in the case of masonry structures. For instance, in Figure 11 the results in terms of elastic behaviour of the numerical model representing the diagonal compression test (discussed in the following subsection), with the elastic material properties identified in (Chisari, et al., 2015) are compared with the experimental data already presented in Section 3.3.1. It is clear that the principal diagonal shortening is severely overestimated, while the secondary diagonal lengthening is correctly captured.

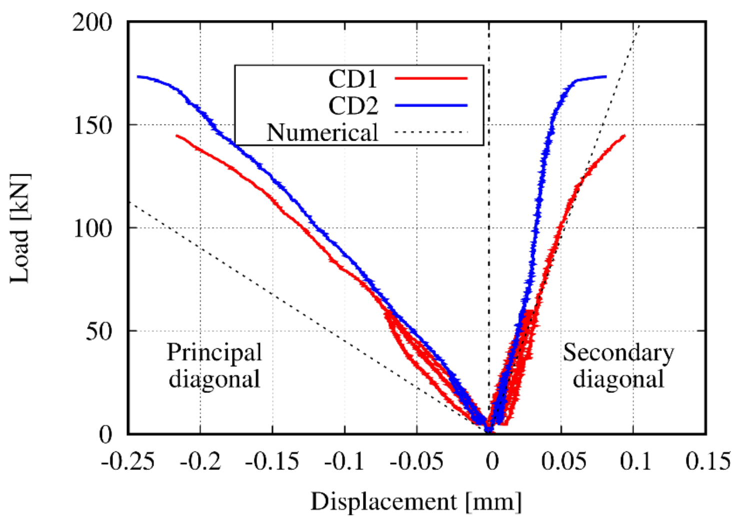

Figure 11. Experimental plots and numerical predictions of the diagonal compression test elastic behaviour using properties calibrated in (Chisari, et al., 2015).

The inaccurate prediction given by the calibration performed in (Chisari, et al., 2015) is due to the intrinsic features of masonry-like materials, which are characterised by very low tensile strength and generally experience initial cracking due to stress concentrations even for low loading levels. Thus, similar to materials not resisting tension, the “apparent” stiffness depends upon the stress state (Angelillo, et al., 2010; Fortunato, 2010). The consequence is that a blind parameter identification performed on a test in which large parts of the structure are subjected to tension (as in the flat-jack test) may provide lower elastic properties than a test in which compression is prevalent (diagonal test). For this reason, the estimation of the elastic parameters for the numerical model simulating the tested masonry was based in this study on the response recorded in the diagonal compression tests. To this aim, the elastic phase was defined as secant stiffness between 20 kN and 60 kN before the onset of cracks in the two specimens. On the contrary, the nonlinear parameters of the model may be determined onto the results of the novel flat-jack test, as described in Section 4.2. It is underlined that the specimens tested according to different protocols and setups in this research were made of the same nominal materials. In real-world applications, a diagonal compressive test is often unfeasible for existing structures, as it would imply complete destruction of the wall. Elastic parameters should be estimated by means of tests in which tensile stress does not play a significant role, as for instance ordinary double flat-jack tests. Different sources of information coming for instance from double-flat-jack tests, micro-drilling, acoustic emissions, operational modal analysis could also be included in a unified strategy exploring the possibilities offered by multi-objective calibration (Chisari, et al., 2017). Another approach, herein not investigated, could consist of performing the calibration of both elastic and strength parameters at the same time, without preliminarily identifying the elastic branch. This would allow the consideration of early-stage cracking and damage even though it is not apparent from the test.

4.1.2 FE modelling

A FE mesoscale model of the test was developed. Each brick was discretised by two 20-noded solid elements connected by stiff elastic 16-node interfaces. Mortar joints were modelled by elastic 16-node interface elements, with vertical and horizontal interfaces having different properties. The two steel angles were represented by very stiff solid elements (E=300GPa) at the top and bottom of the panel; the bottom angle was fully restrained. Four vertical forces F_{00}, F_{01}, F_{10}, F_{11}, 184 and 90 mm spaced in X and Y directions respectively, were applied on the top angle: by changing the magnitude of each relatively to the others, it is possible to simulate accidental eccentricities e_x and e_y, respectively in X and Y directions. Elastic interfaces were used between the angles and the panel to simulate the plaster layer. The full numerical model is displayed in Figure 12a,b. The head joint Young modulus was assumed equal to the bed joint's E_m, multiplied by a factor r less than unity to account for the possible decrease in stiffness due to a reduced bond between units and mortar.

Since each forward analysis lasts a few seconds, the use of surrogate model as described in Section 2.2.2 is not required. Thus, all the optimisation and sensitivity analyses were performed employing the FE description.

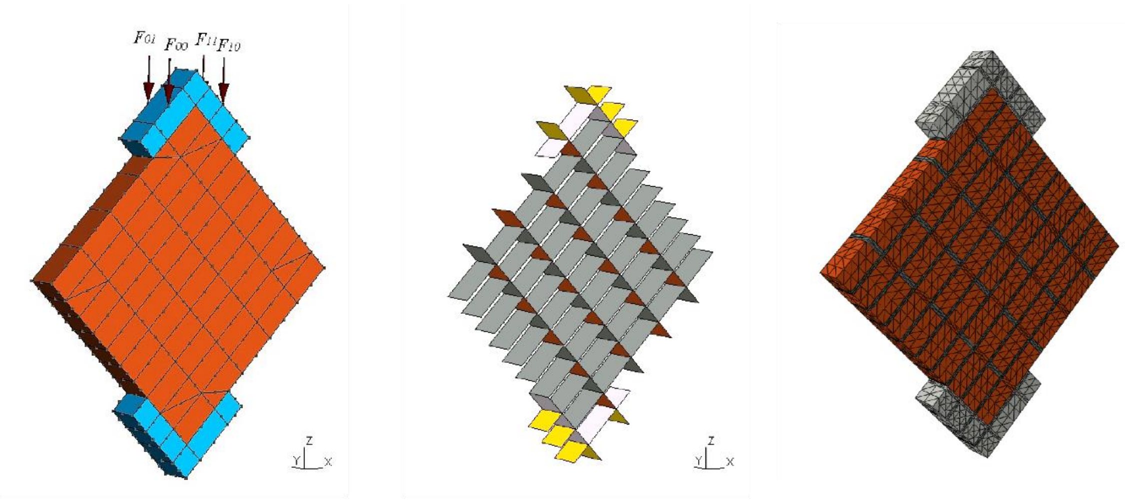

(a) (b) (c)

Figure 12. FE model of the diagonal compression test: (a) view of the mesoscale model, (b) arrangement of interfaces, (c) 3D detailed model.

4.1.3 Verification of mesoscale representation

To verify the validity of the mesoscale framework and discretisation, a detailed 3D model with elastic solid elements for both units and mortar joints and rather fine mesh discretisation was also developed (Figure 12c). This was then used as benchmark to compare the response of the mesoscale model with coarse mesh, and elastic properties defined as in Eqs. (7)-(10). The comparison was performed on several geometrically identical models with different elastic material properties. Thus, 200 samples for both modelling types were generated by varying the main material parameters in the ranges displayed in Table 1 according to Sobol distribution (Antonov & Saleev, 1979). The force F, assumed centred, was fixed at 100kN. The relative displacements of the points corresponding to the instruments 1-7 displayed in Figure 4a were evaluated for both mesoscale and 3D models. The results relative to instruments 1 and 2 are displayed in Figure 13, along with the regression line. It may be noticed that a good agreement between the two representations exists (R>0.95) with very small differences (slope of the tendency line equal to 1.02) for all instruments. Thus it may be argued that the mesoscale representation with two solid elements per brick is sufficiently accurate in the elastic range compared to a more demanding full 3D model.

Table 1. Variation range for the material parameters in the validation of the diagonal compression test model.

Parameter	**Explanation**	**Lower bound**	**Upper bound**
E_b (N/mm2)	Brick Young modulus	5000	20000
E_m (N/mm2)	Mortar Young modulus (bed joint)	5000	30000
r	Head joint Young modulus ratio	0.001	1
ν_b	Brick Poisson's ratio	0.001	0.499
ν_m	Mortar Poisson's ratio	0.001	0.499

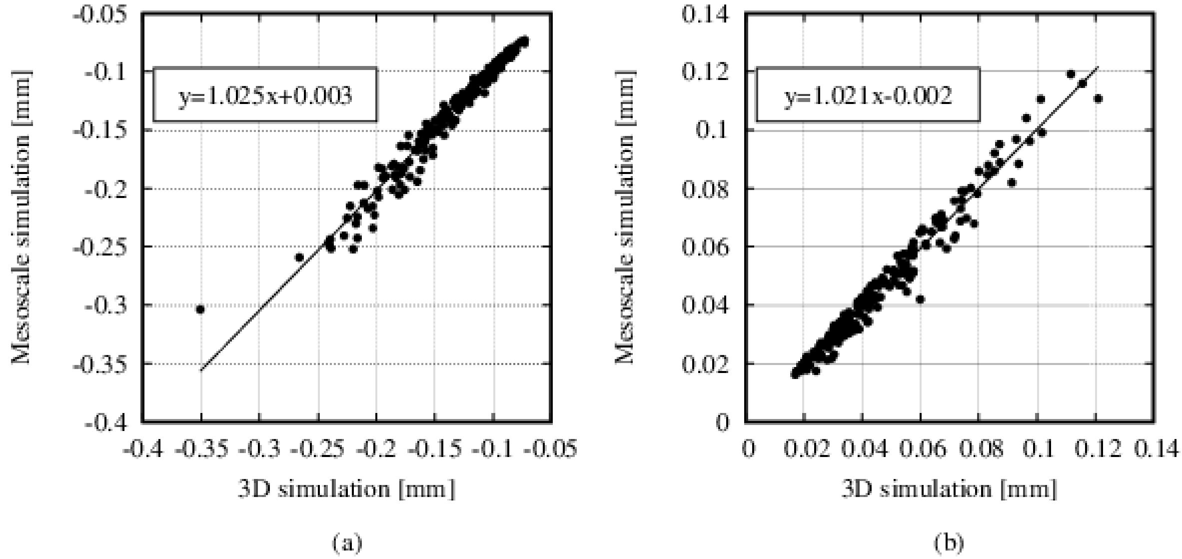

Figure 13. Comparison between 3D and mesoscale model of the diagonal compression test: (a) LVDT 1; (b) LVDT 2.

4.1.4 Sensitivity analysis

The model parameters include:

- Brick parameters: E_b, ν_b;
- Mortar parameters: E_m, ν_m, r;
- Plaster parameters: $k_{N,pl}$, $k_{V,pl}$;
- Boundary conditions: e_x, e_y.

A global sensitivity analysis was performed considering the variation of the parameters above by means of the Elementary Effects Method, as described in Section 2.2.3. Since a strong correlation is expected between E_m and E_b, the mortar parameter considered was the ratio E_m/E_b instead of only E_m. The variation range for the global sensitivity analysis is reported in Table 2. Ten sample points (N=10) were selected according to the procedure proposed in (Campolongo, et al., 2011). The total number of evaluations is thus $N(k+1)$=100, where k=9 is the number of sought parameters. The results in terms of μ_i, σ_i for the L_1-norm of the vector collecting the data corresponding to the 12 LVDTs are displayed in Figure 14. The plot shows that the most influential parameters in the recorded response are e_y, E_b and E_m/E_b, and thus they will be considered as the unknown of the identification problem. All the other parameters lay in an area close to the origin, meaning that their effect can be neglected. For this reason, in the inverse analysis they were assumed as constant, equal to the values reported in Table 3. The plaster axial stiffness was assumed very high compared to shear stiffness to account for early cracking in the layer, which makes the load transferred from the angle to the specimen mainly by normal stresses. The brick Poisson's ratio was set equal to the experimental value, while for the mortar Poisson's ratio a typical value in the literature was considered. Finally, the load was assumed as centred in the x-direction.

Table 2. Variation range for the material parameters in the sensitivity analysis of the diagonal compression test.

Parameter	**Lower bound**	**Upper bound**
E_b (N/mm^2)	5000	20000
ν_b	0.001	0.499
E_m/E_b	0.01	1.5
ν_m	0.001	0.499
r	0.001	1.000
$k_{N,pl}$ (N/mm^3)	1	100
$k_{V,pl}$ (N/mm^3)	1	100
e_x	0.0	1.0
e_y	0.0	1.0

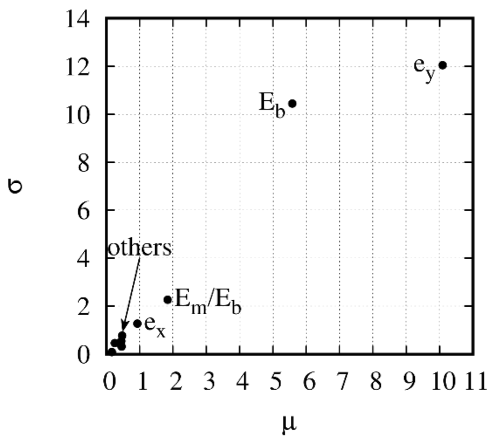

Figure 14. Results of the global sensitivity analysis of the diagonal compression test.

Table 3. Constant parameters for the elastic identification problem.

Parameter	Value
$k_{N,pl}$	50 N/mm^3
$k_{V,pl}$	1 N/mm^3
υ_b	0.187
υ_m	0.2
r	1.0
e_x	0.5

4.1.5 Results of the inverse analysis

The solution $\tilde{\boldsymbol{m}}$ in terms of brick and mortar Young modulus and out-of-plane eccentricity was obtained by solving the following problem for each of the two tests CD1 and CD2:

$$\tilde{\boldsymbol{m}} = \arg\min_{\boldsymbol{m}} \left[\frac{1}{N} \sum_{i=1}^{N} \left| u_{i,exp} - u_{i,c}(\boldsymbol{m}) \right| \right] \tag{17}$$

where N=12 is the number of LVDTs, $u_{i,exp}$ and $u_{i,c}$ the i-th recorded displacement for the experimental test and the numerical model, respectively.

The minimisation of the discrepancy function (17) was carried out by a GA characterised by the following parameters:

- Population: 50 individuals;
- Initial population generated by the Sobol algorithm;
- Number of generations: 100;
- Selection: Stochastic Universal Sampling, with linear ranking and scaling pressure equal to 2.0;
- Crossover: Blend-α, with α=2.0;
- Crossover probability: 1.0;
- Mutation probability: 0.005.

Both the operators and the GA internal variables were selected considering the results of previous research (Chisari, 2015). In particular, quasi-random sequences as the Sobol algorithm explores the parameter space more uniformly than simple random sequence.

Stochastic Universal Sampling avoids the phenomenon of genetic drift; Blend-α crossover with α=2.0 is designed to preserve the probability density function of the population while keeping its ability of yielding novel solutions in the finite population case, e.g. functional specialization hypothesis (Kita & Yamamura, 1999). According to the same principle, the scaling pressure and the number of generations were designed to gradually narrow the probability distribution function of the population. Crossover and mutation probabilities are based on previous research and are consistent with general literature assumptions.

The average of the results between the two tests read E_b=13300MPa and E_m=10100MPa. The brick Young's modulus is slightly higher than the value displayed in Table 1 (19% increase). However, in the literature (Fodi, 2011) it is shown that clay-bricks have higher stiffness and strength along the short direction, while the values shown in Table 1 were estimated by loading the brick along the longest direction (stretcher). Thus, if an isotropic material is used to model actual anisotropic behaviours, as in the mesoscale representation, it must average these differences in properties. Since the mortar Young's modulus was found close to E_b, in the mesoscale approximation (7) and (8) the interface stiffness resulted in very high values, and thus in the elastic phase the masonry may be regarded as a homogeneous material with Young's modulus equal to E_b. The nonlinear properties for mortar-brick interfaces, which are preferential sliding surfaces where the crack starts and propagates, were estimated considering the experimental response of the flat-jack test, as described in the next subsection.

4.2 Nonlinear parameters

4.2.1 The FE model and kriging approximation

A nonlinear FE model of the masonry specimen investigated in the flat-jack test was developed considering a discretisation of the masonry texture following the approach described for the diagonal test. Thus, each brick was represented by two 20-noded solid elements connected by a rigid-plastic 16-noded interface elements. Different interface material properties were used to model head and bed joints. Thanks to the geometrical and loading symmetry, only half specimen was discretised adding appropriate symmetry constraints. In a first phase, the vertical load was applied as distributed load on the top surface of the specimen. Conversely, a specific approach, based on the idea proposed in (Anthoine, 2006), was used to model the load transferred by the flat-jack, with the aim of capturing the post-peak response. In this respect, the force proportional loading was transformed into a displacement-controlled load by inserting constraints at the nodes where the load is applied. A system of statically determined rigid elements allowed the transfer of a uniformly distributed load onto the masonry (Figure 15) capturing the softening branch of the load-displacement curve. To overcome numerical difficulties, dynamic analyses were performed imposing a constant velocity at the node where the displacement is controlled. The Hilber-Hughes-Taylor integration scheme with α=-0.33, β= 0.25(1-α)^2, γ=0.5-α was employed.

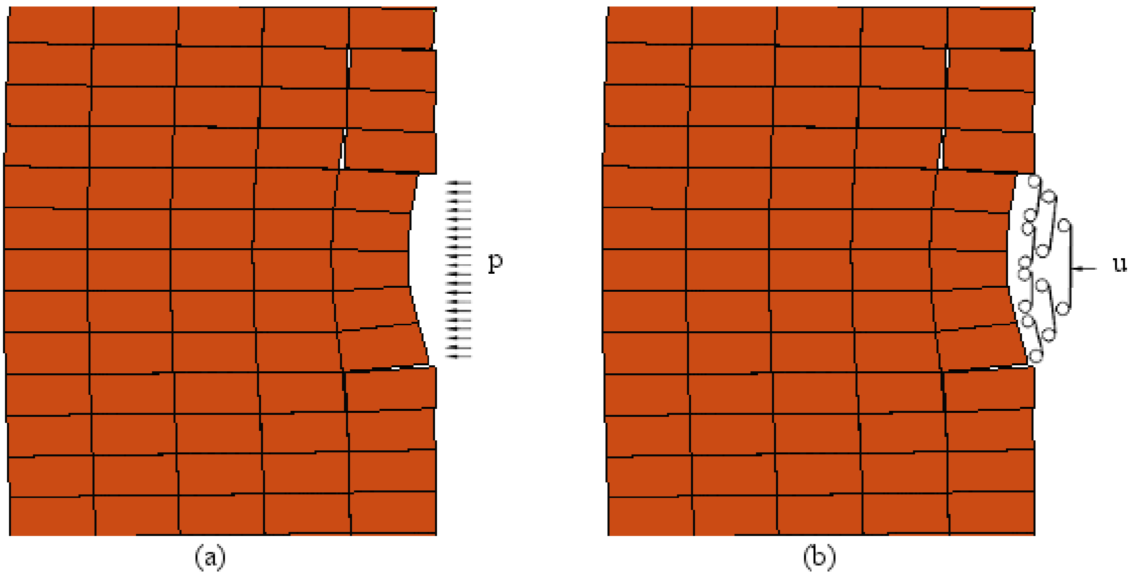

Figure 15. Flat-jack load modelling: (a) force-control; (b) displacement-control.

The elastic properties determined from the diagonal compression tests presented in the previous subsection were assumed. The nonlinear parameters $\boldsymbol{m}$ governing the model response are:

- Brick parameters f_{tb}, $G_{fb,I}$;
- Interface parameters c, $\tan\phi$, σ_t, $G_{f,I}$, $G_{f,II}$.

In the investigation, L=11 load-displacement curves provided by the LVDTs located around the vertical flat-jack were considered (Figure 6); from those, T=3 reference values were extracted, i.e. the effective pressures recorded when each LVDT recorded the displacements δ_1=0.1mm, δ_2=0.325, δ_3=0.8mm, respectively. The calibration was carried out by solving the minimisation problem:

$$\tilde{\boldsymbol{m}} = \arg\min_{\boldsymbol{m}} \sum_{i=1}^{L} \sum_{j=1}^{T} \left| p_{j,c}^{i}(\boldsymbol{m}) - p_{j,exp}^{i} \right| \qquad (18)$$

where p_j^i represents the effective pressure on the flat-jack when the i-th LVDT reaches the j-th displacement reference value. The extraction of $p_{j,exp}^i$ from the load-displacement plot is shown in Figure 16 with reference to LVDT 2 (corresponding to the experimental plot shown in Figure 9); the extraction of $p_{j,c}^i$ is analogous as it is derived from the numerical curve.

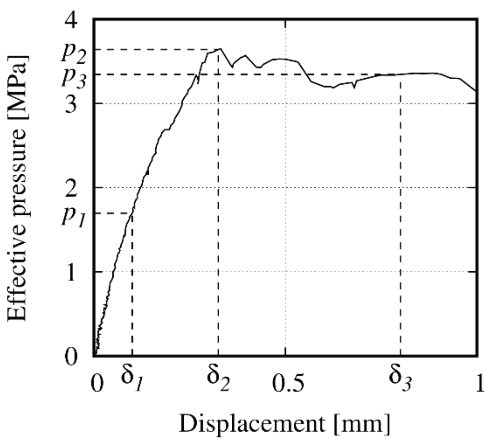

Figure 16. Points to match in the load-displacement plot of LVDT 2 in the flat-jack test.

An efficient metamodel was developed and validated, as the direct use of the 3D mesoscale description described before for the sensitivity analysis and the minimisation of the objective function was impractical, due to the substantial computational cost. A set of 200 design points in the parameter space for the kriging approximation was defined by using the Sobol sequence. The admissible variation ranges for the parameters are reported in Table 4. For each parameter design load-displacement curves were obtained from the results of the expensive FE model. A different kriging metamodel for each $p_{j,c}^{i}$ was built on the 200 design samples. It should be pointed out that not all the design samples were able to converge up to the displacements δ_1, δ_2, δ_3: so the design points for the metamodels were always less than 200; for instance, they were 191, 121, 49, respectively, for the metamodels related to LVDT 2. For this reason, it is expected that the metamodels approximating response p_3 are less accurate than the others, as they were tuned on less design points.

Table 4. Variation range for the strength material parameters.

Parameter	Explanation	Lower bound	Upper bound
f_{tb} (N/mm^2)	Brick tensile strength	0.5	7.0
$G_{fb,I}$ (N/mm^3)	Brick fracture energy (mode I)	0.01	0.25
c (N/mm^2)	Interface cohesion	0.1	1.8
$tan\phi$	Interface friction coefficient	0.45	1.5
σ_t (N/mm^2)	Interface tensile strength	$0.1 \cdot c$	$0.5 \cdot \frac{c}{tan\varphi}$
$G_{f,I}$ (N/mm^3)	Interface fracture energy (mode I)	0.005	0.02
$G_{f,II}$ (N/mm^3)	Interface fracture energy (mode II)	0.01 (with $G_{f,II} > G_{f,I}$)	0.25

The validation of the metamodel was conducted considering a leave-one-out cross-validation (Queipo, et al., 2005) to provide a reliable estimate of the error in the approximation without additional computational cost. In leave-one-out cross validation, the metamodel is trained N separate times (with N=number of design samples) on N-1 design points and a prediction is made for the point not considered in the training. On this set of N predictions, some statistics of the error are computed and used to evaluate the model. This technique was used to select the optimal metamodel for each response p_1, p_2, p_3 among those proposed by the package

DACE by means of a GA managed by TOSCA. The details of the process are not reported for the sake of brevity, but, as an example, the characteristics of the final metamodels adopted for LVDT 2 are reported in Table 5. As expected, the metamodel related to p_3 features higher levels of error compared to the others, due to the smaller number of design points utilised. To increase the confidence in the approximation, more design points reaching the deformation level δ_3 would be necessary, but for the purposes of this investigation the error level given by this metamodel was considered acceptable.

Table 5. Metamodels adopted for approximating reference response quantities for LVDT 2 in the flat-jack test.

Response quantity	Regression model	Correlation model	Error average [%]	Error standard deviation [%]
p_1	Zero order polynomial	Exponential	0.1%	3.6%
p_2	First order polynomial	Gaussian	0.9%	6.6%
p_3	Zero order polynomial	Gaussian	1.8%	14.7%

4.2.2 Sensitivity analysis

Once the metamodels were trained and validated, they were used for sensitivity analysis of the objective function ω employing the elementary effect implemented in the software SAFE (Pianosi, et al., 2015). The parameters and the bounds were those described in Table 4. N=100 sample points were used, and the sensitivity of the L_1-norm of the vector collecting all $p^{i}_{j,c}$ to each input variable was evaluated.

The results are reported in Figure 17, where it can be noticed that the most influential parameters in the nonlinear response are the brick tensile strength f_{tb}, the Mode-II fracture energy $G_{f,II}$, the mortar cohesion c and the friction coefficient $tan\phi$. All the other parameters are less critical and will be considered as constant in the optimisation process. In particular, the values reported in Table 6 were utilised, representing the mean values of the ranges shown in Table 4.

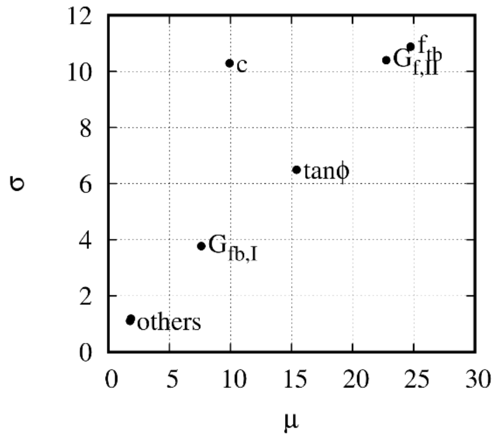

Figure 17. Results of the global sensitivity analysis of the flat-jack test.

Table 6. Constant parameters for the nonlinear identification problem.

Parameter	Value
$G_{fb,I}$ (N/mm^3)	0.1
σ_t (N/mm^2)	$0.05 \cdot c + 0.25 \cdot \frac{c}{tan\varphi}$
$G_{f,I}$ (N/mm^3)	0.01

4.2.3 Results of the inverse analysis

The minimisation of the discrepancy function (18) was carried out by a GA characterised by the same parameters as for the elastic problem described in Section 4.1. The optimal metamodel obtained by the analysis considers the following parameters:

- c=0.32N/mm^2;
- $tan\phi$=1.03;
- f_{tb}=5.3N/mm^2;
- $G_{f,II}$=0.188N/mm^3.

The cohesion, the friction coefficient and the brick tensile strength seem compatible with the values obtained from standard material tests (Table 1), even though f_{tb} is slightly higher than the value evaluated through the splitting test on the bricks. Furthermore, the friction coefficient agrees well with the simplified analysis proposed in (Chisari, et al., 2015) and based on the final state of the test. The Mode-II fracture energy appears similar to the values generally reported in the literature, and it was not possible to estimate it from the tests on triplets, as they were force-controlled.

A full FE model of the test with the optimal material parameters was created in ADAPTIC. The comparison between the experimental and the numerical data are reported in Figure 18, along with the values p_1, p_2, p_3 estimated by the surrogate model.

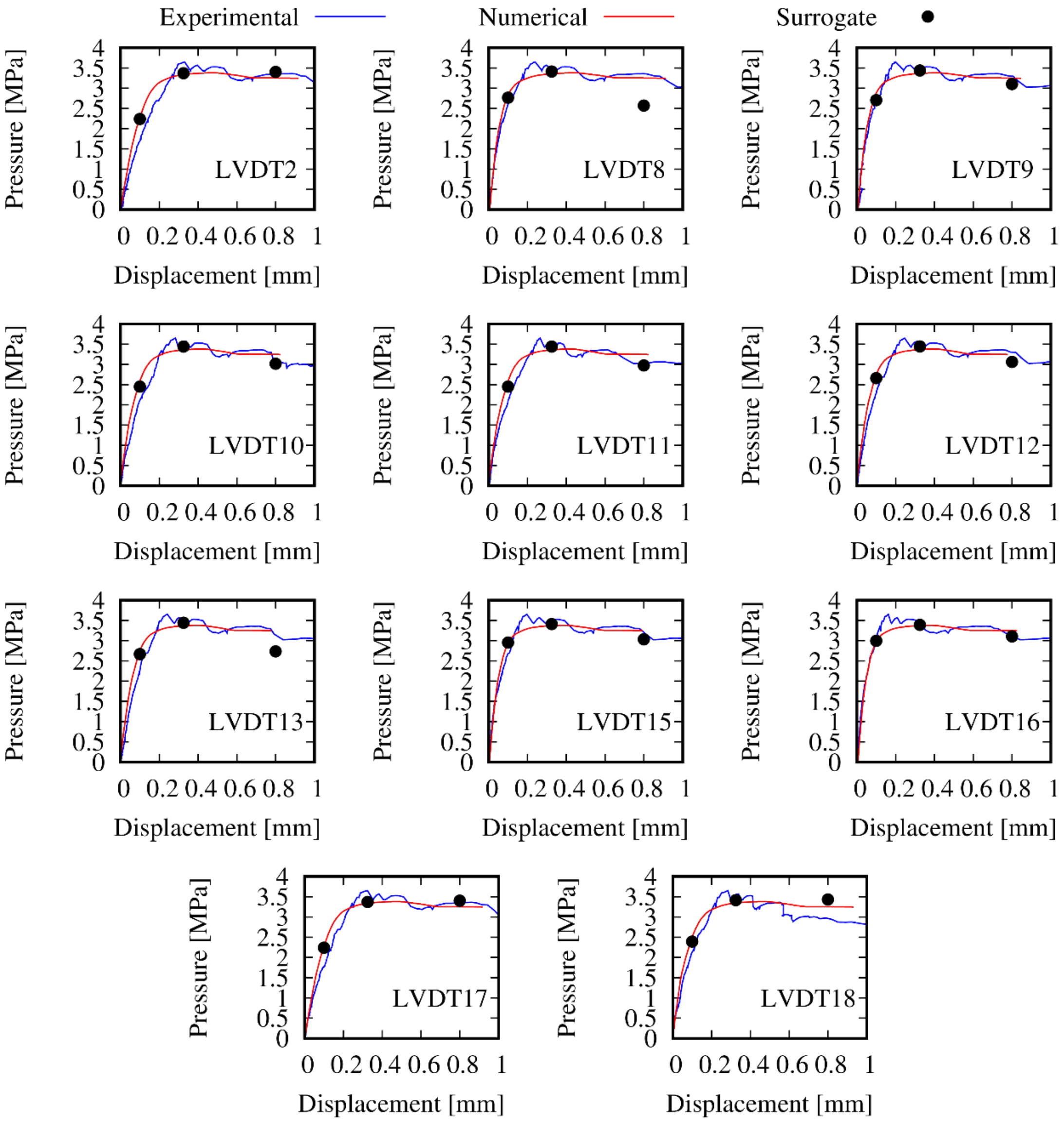

Figure 18. Comparison between experimental and numerical responses for the flat-jack test.

It is observed that the accuracy of the metamodel compared to the expensive FE model is excellent for p_1 and degrades for p_2 and particularly p_3. This was expected from the results of the metamodel validation, as reported in Table 5 for LVDT2. More design points would be needed to build a more accurate surrogate model for p_2 and p_3.

Notwithstanding this lower accuracy of the surrogate model, the agreement between numerical and experimental data is generally good, and thus the result of the inverse analysis, based on the surrogate model, seems reliable. The fitting of the numerical responses is more accurate for LVDT 8, 9, 15, 16, which are located far from the flat-jack (see Figure 6), while the initial stiffness is slightly overestimated for the other instruments. This may indicate that the response near the flat-jack is influenced by local damage as an effect of the cutting.

The deformed shape of the specimen generated by the post-processor Gmsh (Geuzaine & Remacle, 2009), is displayed in Figure 19a-b for the initial and final state respectively, using a scale factor of 100. It shows that the physical crack pattern in Figure 10 is well reproduced by the model. In particular, top diagonal (Mode I and II) cracks may be seen in Figure 19b; Mode I cracks at the external bed joints and bottom quasi-vertical cracks are noticed as well. This is in good agreement with the experimental observations.

An interesting remark concerns the distribution of vertical stresses σ_z depicted in Figure 19. At the beginning of the test all bed joints are subjected to uniform vertical pressure transferred by the steel beam, but during the test the distribution of vertical stresses changes considerably due to the effects of the vertical pressure at flat-jack load and stress distribution due to cracking. This leads to the development of tension in the bed joints at the external parts of the wall which also implies that the vertical stresses are not uniform on the bed joints of the specimen. On one side, this confirms what was pointed out in Section 4.1.1 about the presence of tensile stresses in this test. On the other side, the variable stress distribution enables the estimation of the friction angle together with the cohesion, because more (σ_v-τ)

couples are available to implicitly fit the failure surface. This avoids resorting to the simplified approach described in (Chisari, et al., 2015) which needs a fully damaged specimen.

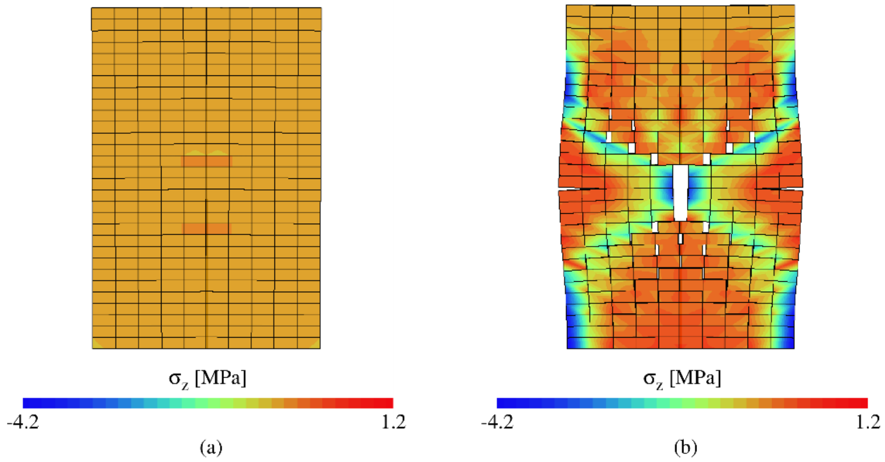

Figure 19. Results of the numerical model of the flat-jack test: deformed shape(a) at the initial state, and (b) at failure. The contour plot of the vertical stress σ_z is superimposed.

4.2.4 Some remarks on computational time

The computational time required to perform a single elastic analysis of the diagonal compression test is about 9s. Considering the population size and number of generations described in Section 4.1.5 and the possibility that an individual may appear more than once during the optimisation process (but will not be evaluated again), the complete identification analysis lasted ~12 hours. On the contrary, the single nonlinear analysis of the flat-jack test requires much more time which in turn depends on the particular combination of parameters. The 200 FE analyses performed for the construction of the metamodel were on average 4.76 hours long, including a maximum analysis time of 23.75 hours. Thanks to the availability of High Performance Computing facilities at Imperial College London, it was possible to run them mostly in parallel, and completing the design point evaluation in a few days, but the impossibility of an optimisation analysis based on the full FE model is evident. After its calibration, the metamodel ran in about 3s and the complete characterisation of the nonlinear parameters was completed in ~4 hours.

5 Conclusions

In this work, an experimental-numerical procedure is proposed for the identification of material parameters of an accurate mesoscale masonry model. This is based on the inverse analysis of the experimental data provided by tests on small panels and walls. In particular, the elastic parameters are estimated from the output of diagonal compression tests, while nonlinear parameters from a purposely designed flat-jack test. The procedure involves the minimisation of a functional of the discrepancy between experimental outcomes and numerical simulation provided by the FE model of the test. When this becomes excessively demanding, it is proposed to use a validated metamodel in place of the expensive FE model.

The results of the inverse analysis, which have been conducted after a sensitivity analysis leading to a reduction of the sought material parameters, confirm that the proposed approach enables an accurate calibration of the main model material parameters.

One of the main merit of the developed methodology regards the practicality of the proposed in-situ test which is simple and low-invasive. Moreover, the material parameter identification is based on processing basic experimental data (e.g. relative displacements). The main demand of the method mainly resides in the post-processing phase, where a sensitivity analysis and optimisation process are carried out after developing and validating detailed FE descriptions and associated surrogate models. Each of these sub-phases has been addressed in this paper carefully considering (i) the computational cost of the numerical analysis, (ii) the reliability of the surrogate model, (iii) the selection of the material parameters to be realistically calibrated given the experimental data, and (iv) optimisation issues.

The application of the identification procedure to physical experiments allowed some critical considerations related to the general methodology and the proposed flat-jack test which may lead to future improvements for the proposed calibration strategy. The experimental results confirm that it is very difficult to identify an “elastic” phase in the response, as linear load-displacement curves may erroneously be considered as elastic while in fact they are related to a situation in which some damage has already developed. In this research, the elastic properties were identified using the diagonal compression test, which is actually rather complicated to perform in-situ. These difficulties could be avoided if a separation between the elastic and nonlinear branches is not artificially set, and all parameters, elastic and nonlinear, are identified together by the same flat-jack test. Evidently, this would require the execution of a larger number of numerical simulations, where the use of metamodels may mitigate the computational cost enhancing efficiency. About the practical implementation of the flat-jack test, the use of local reinforcement to avoid undesirable Mode-I failure in the bricks appears feasible. For practical in-situ applications, it is also expected that the distance of the flat-jack from the openings may influence the activation of different failure modes, and thus it is suggested to perform the test in situ under several conditions to estimate more parameters. Based on the results of this investigation, it is also recommended to place the instrumentation rather far from the flat-jack, to decrease the influence of local defects. Further research will focus on the improvement of the procedure following these guidelines and on the application to real structures.

Acknowledgements

The authors are grateful to Dr Franco Trevisan and the laboratory staff at the University of Trieste for the technical support during the experimental programme, as well as to Prof. Natalino Gattesco and Mr. Enrico Zanello on behalf of FibreNet s.r.l. for supplying and advising on CFRP application. Ms Elisa Widmar's support for some illustrations is also acknowledged. The authors are grateful to Dr Pianosi from the University of Bristol for helpful advice regarding SAFE software. The authors also acknowledge the Research Computing Service at Imperial College for providing and supporting the required High Performance Computing facilities.

References

Angelillo, M., Cardamone, L. & Fortunato, A., 2010. A numerical model for masonry-like structures. *Journal of Mechanics of Materials and Structures,* 5(4), pp. 583-615.

Anthoine, A., 1995. Derivation of the in-plane elastic characteristics of masonry through homogenization theory. *International Journal of Solids and Structures*, 32(2), pp. 137-163.

Anthoine, A., 2006. A simple displacement control technique for pushover analyses. *Earthquake Engng Struct. Dyn.,* Volume 35, pp. 851-866.

Antonov, I. A. & Saleev, V. M., 1979. An economic method of computing LP tau-sequence. *USSR Computational Mathematics and Mathematical Physics,* 19(1), pp. 252-256.

ASTM, 1991. *In-situ compressive stress within solid unit masonry estimated using flat-jack measurements,* s.l.: ASTM Standard C 1196-91.

Atkinson, R. H., Amadei, B. P., Saeb, S. & Sture, S., 1989. Response of masonry bed joints in direct shear. *Journal of Structural Engineering,* 115(9), pp. 2276-2296.

Berto, L., Saetta, A., Scotta, R. & Vitaliani, R., 2002. An orthotropic damage model for masonry structures. *Int J Numer Methods Eng,* Volume 55, pp. 127-157.

Brencich, A. & de Felice, G., 2009. Brickwork under eccentric compression: Experimental results and macroscopic models. *Construction and Building Materials,* 23(5), pp. 1935-1946.

BS 5628-1: 2005, 2005. *Code of practice for the use of masonry. Part 1: Structural use of unreinforced masonry.* s.l.:British Standard.

Calderini, C., Cattari, S. & Lagomarsino, S., 2010. The use of the diagonal compression test to identify the shear mechanical parameters of masonry. *Construction and Building Materials,* Volume 24, p. 677–685.

Caliò, I., 2011. *La prova di scorrimento con martinetto piatto.* Bari (Italy), Proceedings of the Fourteen Conference ANIDIS.

Campolongo, F., Saltelli, A. & Cariboni, J., 2011. From screening to quantitative sensitivity analysis. A unified approach. *Computer Physics Communications,* Volume 182, pp. 978-988.

Chaimoon, K. & Attard, M., 2007. Modeling of unreinforced masonry walls under shear and compression. *Engineering Structures,* 29(9), pp. 2056-2068.

Chiozzi, A., Milani, G. & Tralli, A., 2017. A Genetic Algorithm NURBS-based new approach for fast kinematic limit analysis of masonry vaults. *Computers & Structures,* Volume 182, pp. 187-204.

Chisari, C., 2015. *Inverse techniques for model identification of masonry structures.* University of Trieste: PhD Thesis.

Chisari, C. & Bedon, C., 2016. Multi-objective optimization of FRP jackets for improving seismic response of reinforced concrete frames. *American Journal of Engineering and Applied Sciences,* 9(3), pp. 669-679.

Chisari, C. et al., 2017. Critical issues in parameter calibration of cyclic models for steel members. *Engineering Structures,* Volume 132, pp. 123-138.

Chisari, C., Macorini, L., Amadio, C. & Izzuddin, B. A., 2015. *An Experimental-Numerical Procedure for the Identification of Mesoscale Material Properties for Brick-Masonry.* Prague, Civil-Comp Press, Stirlingshire, Scotland.

Chisari, C., Macorini, L., Amadio, C. & Izzuddin, B. A., 2015. An Inverse Analysis Procedure for Material Parameter Identification of Mortar Joints in Unreinforced Masonry. *Computers & Structures,* Volume 155, pp. 97-105.

Chisari, C., Macorini, L., Amadio, C. & Izzuddin, B. A., 2016. Optimal sensor placement for structural parameter identification. *Structural and Multidisciplinary Optimization.*

Claerbout, J. f. & Muir, F., 1973. Robust modeling with erratic data. *Geophysics,* 38(5), pp. 826-844.

CUR, 1994. *Structural masonry: a experimental/numerical basis for practical design rules,* Gouda, The Netherlands: CUR.

Da Porto, F., Guidi, G., Garbin, E. & Modena, C., 2010. In-plane behavior of clay masonry walls: Experimental testing and finite-element modeling. *Journal of Structural Engineering,* 136(11), pp. 1379-1392.

D'Ambrisi, A., Mariani, V. & Mezzi, M., 2012. Seismic assessment of a historical masonry tower with nonlinear static and dynamic analyses tuned on ambient vibration tests. *Engineering Structures,* Volume 36, pp. 210-219.

DRC Diagnostic Research Company, 2015. *http://www.drcitalia.it.* [Online].

Fedele, R., Maier, G. & Whelan, M., 2006. Stochastic calibration of local constitutive models through measurements at the macroscale in heterogeneous media. *Computer Methods in Applied Mechanics and Engineering,* 195(37-40), pp. 4971-4990.

Fodi, A., 2011. Effects influencing the compressive strength of a solid, fired clay brick. *Periodica Polytechnica: Civil Engineering,* 55(2), pp. 117-128.

Fortunato, A., 2010. Elastic Solutions for Masonry-like Panels. *Journal of Elasticity,* Volume 98, pp. 87-110.

Gambarotta, L. & Lagomarsino, S., 1997. Damage models for the seismic response of brick masonry shear walls. Part I: the mortar joint model and its applications. *Earthquake Engineering and Structural Dynamics,* 26(4), pp. 423-439.

Gambarotta, L. & Lagomarsino, S., 1997. Damage models for the seismic response of brick masonry shear walls. Part II: The continuum model and its applications. *Earthquake Engineering and Structural Dynamics*, 26(4), pp. 441-462.

Ganz, H., 1985. *Masonry Walls Subjected to Normal and Shear Forces.* Institute of Structural Engineering, ETH Zurich: PhD Thesis.

Garbowski, T., Maier, G. & Novati, G., 2011. Diagnosis of concrete dams by flat-jack tests and inverse analyses based on proper orthogonal decomposition. *Journal of Mechanics of Materials and Structures,* Volume 6, pp. 181-202.

Gentile, C. & Saisi, A., 2007. Ambient vibration testing of historic masonry towers for structural identification and damage assessment. *Construction and Building Materials,* 21(6), pp. 1311-1321.

Geuzaine, C. & Remacle, J.-F., 2009. Gmsh: a three-dimensional finite element mesh generator with built-in pre- and post-processing facilities. *International Journal of Numerical Methods in Engineering,* Volume 79, pp. 1309-1331.

Goldberg, D. E., 1989. *Genetic Algorithms in Search, Optimization and Machine Learning.* s.l.:Addison-Wesley.

Izzuddin, B. A., 1991. *Nonlinear dynamic analysis of framed structures.* Imperial College London: PhD Thesis.

Jokhio, G. A. & Izzuddin, B. A., 2015. A Dual Super-Element Domain Decomposition Approach for Parallel Nonlinear Finite Element Analysis. *International Journal for Computational Methods in Engineering Science and Mechanics,* 16(3), pp. 188-212.

Kaushik, H., Rai, D. & Jain, S., 2007. Stress-strain characteristics of clay brick masonry under uniaxial compression. *Journal of Materials in Civil Engineering*, 19(9), pp. 728-739.

Kita, H. & Yamamura, M., 1999. *A functional specialization hypothesis for designing genetic algorithms.* s.l., Systems, Man, and Cybernetics, 1999. IEEE SMC'99 Conference Proceedings, pp. 579-584.

Kouznetsova, V., Geers, M. G. D. & Brekelmans, W. A. M., 2002. Multi-scale constitutive modelling of heterogeneous materials with a gradient-enhanced computational homogenization scheme. *International Journal for Numerical Methods in Engineering,* 54(8), pp. 1235-1260.

Lophaven, S. N., Nielsen, H. B. & Søndergaard, J., 2002. *Aspects of the Matlab toolbox DACE, IMM-REP-2002-13,* Kongens Lyngby – Denmark: Technical University of Denmark.

Lophaven, S. N., Nielsen, H. B. & Søndergaard, J., 2002. *DACE - A Matlab Kriging Toolbox,* s.l.: Technical University of Denmark.

Lotfi, H. R. & Shing, P., 1994. Interface model applied to fracture of masonry structures. *Journal of structural engineering,* 120(1), pp. 63-80.

Lourenço, P., 1996. *Computational strategies for masonry structures.* Technische Universiteit Delft: PhD Thesis.

Lourenço, P. B. & Rots, J. G., 1997. Multisurface Interface Model for Analysis of Masonry Structures. *Journal of Engineering Mechanics,* 123(7), pp. 660-668.

Luciano, R. & Sacco, E., 1997. Homogenization technique and damage model for old masonry material. *International Journal of Solids and Structures,* 34(24), pp. 3191-3208.

Macorini, L. & Izzuddin, B., 2011. A non-linear interface element for 3D mesoscale analysis of brick-masonry structures. *International Journal of Numerical Methods in Engineering,* Volume 85, pp. 1584-1608.

Macorini, L. & Izzuddin, B. A., 2013. *Enhanced mesoscale partitioned modelling for unreinforced masonry structures.* Cagliari (Italy), Civil-Comp Proceedings.

Mann, W. & Muller, H., 1982. Failure of shear-stressed masonry. An enlarged theory, tests and application to shear walls. *Proc. Br. Ceram. Soc.,* Volume 30, p. 223.

Massart, T., Peerlings, R. & Geers, M., 2007. An enhanced multi-scale approach for masonry wall computations with localization of damage. *International Journal for Numerical Methods in Engineering,* 69(5), pp. 1022-1059.

McNary, W. & Abrams, D. P., 1985. Mechanics of Masonry in Compression. *Journal of Structural Engineering,* 111(4), pp. 857-870.

Milani, G. & Benasciutti, D., 2010. Homogenized limit analysis of masonry structures with random input properties: polynomial Response Surface approximation and Monte Carlo simulations. *Structural Engineering and Mechanics,* 34(4), pp. 417-447.

Milani, G., Lourenço, P. & Tralli, A., 2006. Homogenised limit analysis of masonry walls, Part I: Failure surfaces. *Computers and Structures,* Volume 84, pp. 166-180.

Mistler, M., Anthoine, A. & Butenweg, C., 2007. In-plane and out-of-plane homogenisation of masonry. *Computers & Structures,* 85(17-18), pp. 1321-1330.

Mojsilovic, N. & Marti, P., 1997. Strength of Masonry Subjected to Combined Actions. *ACI Structural Journal,* 94(6), pp. 633-642.

Morbiducci, R., 2003. Non-linear parameter identification of models for masonry. *Int J Solids Struct,* 40(15), pp. 4071-4090.

Morris, M., 1991. Factorial sampling plans for preliminary computational experiments. *Technometrics,* 33(2), pp. 161-174.

Pantò, B., Cannizzaro, F., Caddemi, S. & Caliò, I., 2016. 3D macro-element modelling approach for seismic assessment of historical masonry churches. *Advances in Engineering Software,* Volume 97, pp. 40-59.

Papa, E., 1996. Unilateral damage model for masonry based on a homogenization procedure. *Mech Cohes-Frict Mater,* Volume 1, pp. 349-366.

Park, K. C. & Felippa, C. A., 2000. A variational principle for the formulation of partitioned structural systems. *International Journal for Numerical Methods in Engineering,* 47(1-3), pp. 395-418.

Pianosi, F., Sarrazin, F. & Wagener, T., 2015. A Matlab toolbox for Global Sensitivity Analysis. *Environmental Modelling & Software,* Volume 70, pp. 80-85.

Poh'sie, G. et al., 2016. Application of a translational Tuned Mass Damper designed by means of Genetic Algorithms on a multistory Cross-Laminated Timber building. *Journal of Structural Engineering,* 142(4), p. E4015008.

Press, W. H., Teukolsky, S. A., Vetterling, W. T. & Flannery, B. P., 2007. *Numerical recipes: the art of scientific computing.* 3rd ed. New York: Cambridge University Press.

Queipo, N. et al., 2005. Surrogate-based analysis and optimization. *Progress in Aerospace Sciences,* 41(1), pp. 1-28.

Sarhosis, V., 2016. Optimisation procedure for material parameter identification for masonry constitutive models. *International Journal of Masonry Research and Innovation,* 1(1), pp. 48-58.

Sarhosis, V. & Sheng, Y., 2014. Identification of material parameters for low bond strength masonry. *Engineering Structures,* Volume 60, pp. 100-110.

Tarantola, A., 2005. *Inverse problem theory and methods for model parameter estimation.* s.l.:SIAM.

UNI EN 1052-3:2007, 2007. *Methods Of Test For Masonry - Part 3: Determination Of Initial Shear Strength.* s.l.:Ente Nazionale di Unificazione.

Xavier, F., Macorini, L. & Izzuddin, B., 2013. *Mesoscale modelling of masonry structures accounting for brick-Mortar interaction.* Cagliari (Italy), s.n.